Chapter 2: Low-Spin d^5 Iron Imides: Nitrene Capture by Low-Coordinate Iron(I) Provides the 4-Coordinate Fe(III) Complexes $[PhB(CH_2PPh_2)_3]Fe{\equiv}NR$

The text in this chapter is reproduced in part with permission from:

Brown, S. D.; Betley, T. A.; Peters, J. C. *J. Am. Chem. Soc.* **2003,** *125,* 322.

2.1 Introduction

While metalloenzymes such as nitrogenases and hydrogenases are far from mechanistically well understood, it seems plausible that low-valent, sulfur-ligated Fe(II) and Fe(I) species play a critical role in their small-molecule reduction chemistry.[1] The careful preparation and study of the redox reactivity of low-coordinate Fe(I) species is therefore of concern.[2,3] Iron(I) is an unusual oxidation state whose coordination chemistry, particularly for low-coordinate examples (4-coordinate or lower), is poorly developed. This point was underscored recently in Parkin's report of the 4-coordinate Fe(I) complex $[PhTp^{tBu}]Fe(CO)$ ($[PhTp^{tBu}]$ = phenyl tris(3-*tert*-butylpyrazolyl)borate).[4] Knowledge of the elementary reactivity patterns of Fe(I) will guide mechanistic postulates for its possible role in biological systems.

This chapter describes metallation of the $[PhBP_3]$ ligand ($[PhBP_3]$ = $[PhB(CH_2PPh_2)_3]^-$)[5] to generate the 4-coordinate Fe(II) halide species, $[PhBP_3]FeX$ (X = Cl, Br, I). Of particular interest is the one electron reduction of the chloride derivative to yield the rare, 4-coordinate Fe(I) species, $[PhBP_3]Fe(PPh_3)$, which serves as a synthetic surrogate to the tripodal "$[PhBP_3]Fe(I)$" subunit. This system undergoes rapid oxidation in the presence of organic azides to produce mononuclear, terminally bound Fe(III) imides, $[PhBP_3]Fe\equiv NR$ (R = alkyl, aryl). Synthetically rare iron oxo and imide/nitrene species continue to receive intense scrutiny due to their postulated role in catalysis.[6,7,8] Recent work by Lee and co-workers provided important precedent for the "Fe=NR" multiple-bond linkage.[6c] However, Lee's system, $[Fe_4(\mu_3\text{-}N^tBu)_4(N^tBu)Cl_3]$, is synthetically ill-defined and electronically complex owing to its cluster nature, which features four magnetically coupled iron centers. The title complexes reported herein provide distinctly simple, mononuclear 4-coordinate Fe(III) imides. Their $S = {}^{1}/_{2}$ ground-state electronic configurations are also distinct in that, to the best of our knowledge, low-spin examples of tetrahedral or pseudotetrahedral Fe(III) were previously unknown.

2.2 Results

2.2.1 Synthesis and Characterization of [PhBP$_3$]FeX (X = Cl, Br, I)

High-yield (>80%) entry into the "[PhBP$_3$]Fe" system proceeded from metallation of FeX$_2$ salts (X = Cl, Br, I) by [Tl][PhBP$_3$][9] to produce the yellow, 4-coordinate high-spin halide derivatives [PhBP$_3$]FeCl (**2.1**), [PhBP$_3$]FeBr (**2.2**), and [PhBP$_3$]FeI (**2.3**) (Equation 2.1). All three halides give rise to characteristic, yet paramagnetically shifted, ^{1}H NMR spectra. Room temperature Evans method magnetic measurements[10] yielded μ_{eff} values of 5.04 μ_B, 5.20 μ_B, and 5.03 μ_B, respectively, consistent with four unpaired electrons (S = 2). UV-vis data correlates with the halide ligand field strengths of the spectrochemical series ($\lambda_{\max}$ = 416 nm (**2.1**), 424 nm (**2.2**), and 438 nm (**2.3**)).[11]

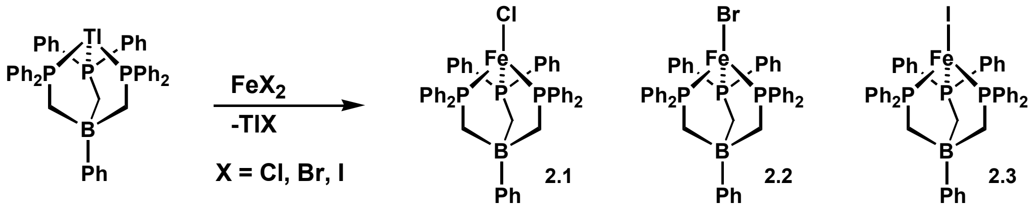

(2.1)

Chloride **2.1** was characterized in the solid state by X-ray crystallography (Figure 2.1) and is rigorously monomeric despite being coordinatively unsaturated and a 14-electron species. This is in direct contrast with the analogous [PhBP$_3$]CoCl[12] and [PhBP$_3$]RuCl[13] species, for which X-ray diffraction experiments yielded dimeric structures. Chloride **2.1** features an Fe-Cl bond distance of 2.2048(10) Å, with Fe-P bond distances of approximately 2.43 Å. The P-Fe-P bond angles average 92°, which is consistent with the description of [PhBP$_3$] as a *facially* capping ligand that occupies one half of an octahedral coordination sphere. The electronic consequences of such a 4-coordinate environment versus that for a rigorously tetrahedral system (*i.e.*, L-M-L = 109.5°) are discussed in Section 2.3. Other threefold symmetric ligand environments such as tris(pyrazolyl)borate,[14] tris(thioether)borate,[15] and triphos ($CH_3C(CH_2Ph_2)_3$)[16] are also known to ligate Fe(II) in a *facially* capping orientation, but only with bulky tris(pyrazolyl)borate ligands have 4-coordinate systems been realized.[4,17] Riordan's tris(thioether)borates, for example, form octahedral species in which the metal center is coordinated by two ligands.[15a]

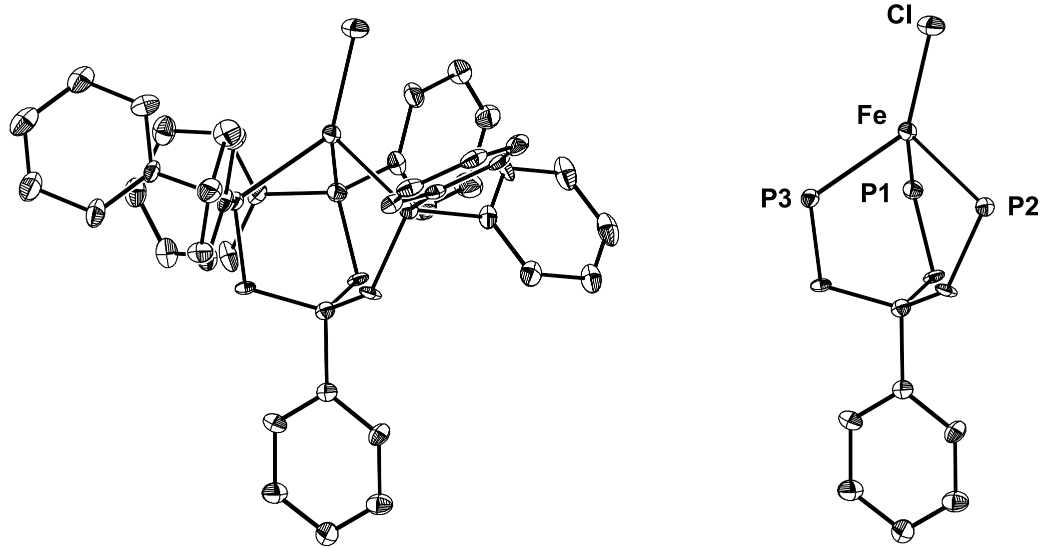

Figure 2.1. 50% thermal ellipsoid representation of [$PhBP_3$]FeCl (**2.1**). For the image on the right, all phosphino phenyl groups have been removed for clarity. For both images, all hydrogen atoms and a benzene solvent molecule have been removed for clarity. Selected bond lengths (Å) and angles (°): Fe-Cl, 2.2048(10); Fe-P1, 2.4318(11); Fe-P2, 2.4168(11); Fe-P3, 2.4268(9); P1-Fe-P2, 94.29(4); P1-Fe-P3, 89.76(3); P2-Fe-P3, 93.19(4); Cl-Fe-P1, 129.60(4); Cl-Fe-P2, 110.57(4); Cl-Fe-P3, 129.63(4).

Little structural difference is observed between **2.1** and the second generation high-spin chloride, $[PhBP^{iPr}_3]FeCl$ ($[PhBP^{iPr}_3] = [PhB(CH_2P^iPr_2)_3]^-$; Fe-Cl = 2.220(1) Å; $Fe\text{-}P_{avg.}$ = 2.42 Å; $P\text{-}Fe\text{-}P_{avg.}$ = 94°).[13] The largest deviation is manifested in the Cl-Fe-P bond angles, which are approximately 110°, 129°, and 129° for **2.1**, and 122° for all three angles of $[PhBP^{iPr}_3]FeCl$. Electronically, a comparative cyclic voltammetry study between the two species reveals a significant difference in the potential of the $Fe^{I/II}$ redox couple. As shown in Figure 2.2, a fully reversible, one-electron redox event is observed at -1.65 V versus Fc/Fc^+ for **2.1**. This potential is approximately 320 mV more positive than that observed for $[PhBP^{iPr}_3]FeCl$,[13] which is presumably due to the weaker σ-donating and better π-accepting properties of aryl versus alkyl phosphine ligands.

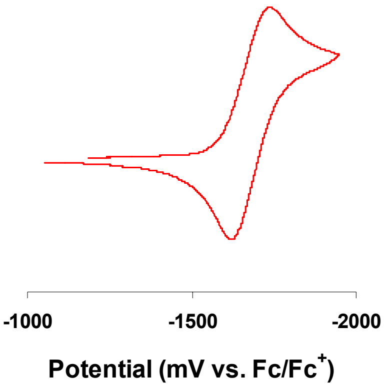

Figure 2.2. Cyclic voltammetry of $[PhBP_3]FeCl$ (**2.1**) (THF, 0.4 M [TBA][PF_6], scan rate = 50 mV/s).

2.2.2 Synthesis and Characterization of $[PhBP_3]Fe(PPh_3)$

As anticipated from the aforementioned electrochemical data, chloride **2.1** was readily reduced by one electron with a sodium/mercury amalgam (THF) in the presence of a triphenylphosphine cap. The desired iron(I) product, $[PhBP_3]Fe(PPh_3)$ (**2.4**), was obtained as an orange, crystalline solid in 62% yield. Repeating the reduction in the absence of triphenylphosphine invariably led to decomposition[18] while the use of PMe_3 resulted in low yields of the desired Fe(I) adduct, impeding its use as a readily available synthetic precursor.

Complex **2.4** features characteristic resonances in the ^1H NMR spectrum and a high-spin electronic ground-state at room temperature ($\mu_{eff} = 3.88\ \mu_B$, $S = {}^3/_2$). X-ray crystallography (Figure 2.3) established a 4-coordinate, pseudotetrahedral geometry in which the P_{borate}-Fe-P_{borate} bond angles average 96°. The triphenylphosphine ligand was located at a distance of 2.2889(9) Å from the metal center, while the observed Fe-P_{borate} distances of approximately 2.34 Å are ~ 0.1 Å shorter than those of **2.1**.

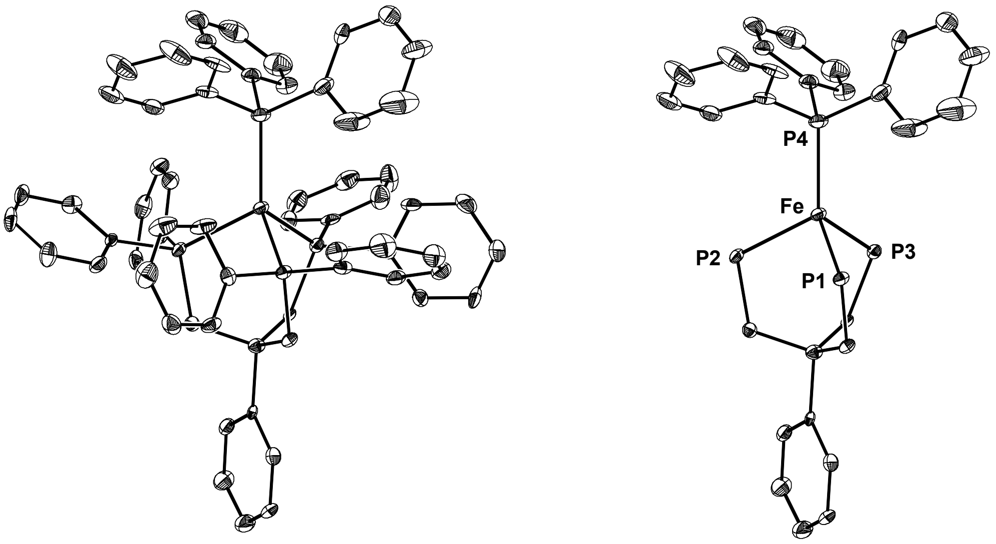

Figure 2.3. 50% thermal ellipsoid representation of $[PhBP_3]Fe(PPh_3)$ (**2.4**). For the image on the right, all phosphino phenyl groups have been removed for clarity. For both images, all hydrogen atoms and disordered solvent molecules have been removed for clarity. Selected bond lengths (Å) and angles (°): Fe-P1, 2.3350(10); Fe-P2, 2.3400(10); Fe-P3, 2.3341(10); Fe-P4, 2.2889(9); P1-Fe-P2, 97.54(3); P1-Fe-P3, 95.58(3); P2-Fe-P3, 96.19(3); P4-Fe-P1, 121.60(4); P4-Fe-P2, 118.79(3); P4-Fe-P3, 121.30(4).

2.2.3 Synthesis and Characterization of Terminal Fe(III) Imides via Oxidative Group Transfer

As demonstrated in Equation 2.2, complex **2.4** underwent clean oxidation by *p*-tolyl azide at room temperature in benzene to provide the forest-green, d^5 imido complex $[PhBP_3]Fe{\equiv}N$-*p*-tolyl (**2.5**), which could be crystallized (50% isolated) by vapor diffusion of petroleum ether into the reaction solution. The overall reaction appeared to be quantitative by ^1H and ^{31}P NMR spectroscopies: a stoichiometric equivalent of *p*-tolyl-N=PPh_3 was produced as the only detectable byproduct. Complex **2.5** was thoroughly characterized by X-ray diffraction (Figure 2.4), SQUID magnetization (Figure 2.5a), EPR spectroscopy (Figure 2.5b), and cyclic voltammetry (Figure 2.5c).

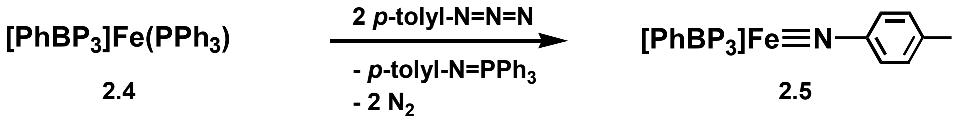

(2.2)

The Fe(1)-N(1)-C(46) bond angle in **2.5** is 169.96(2)°, and the Fe(1)-N(1) bond distance of 1.6578(2) Å is much shorter than typical Fe-amido linkages[19] and is similar to that reported by Lee (1.635(4) Å).[6c] These structural data are consistent with strong π-bonding in the Fe(1)-N(1) linkage: **2.5** is best represented with a triple bond. The axial π-interactions destabilize two orbitals of d_{xz} and d_{yz} parentage to provide the low-spin $S = {}^1/_2$ configuration observed for **2.5,** as indicated from its SQUID magnetization data. For comparison, SQUID data for **2.1** and **2.4** are also presented in Figure 2.5a. All three compounds display temperature independent data in the region 10 to 310 K that obeys the Curie-Weiss law,[20] with effective moments of 5.00, 4.11, and 2.07 μ_B for the $S = 2$, $S = {}^3/_2$, and $S = ½$ systems, respectively.[21]

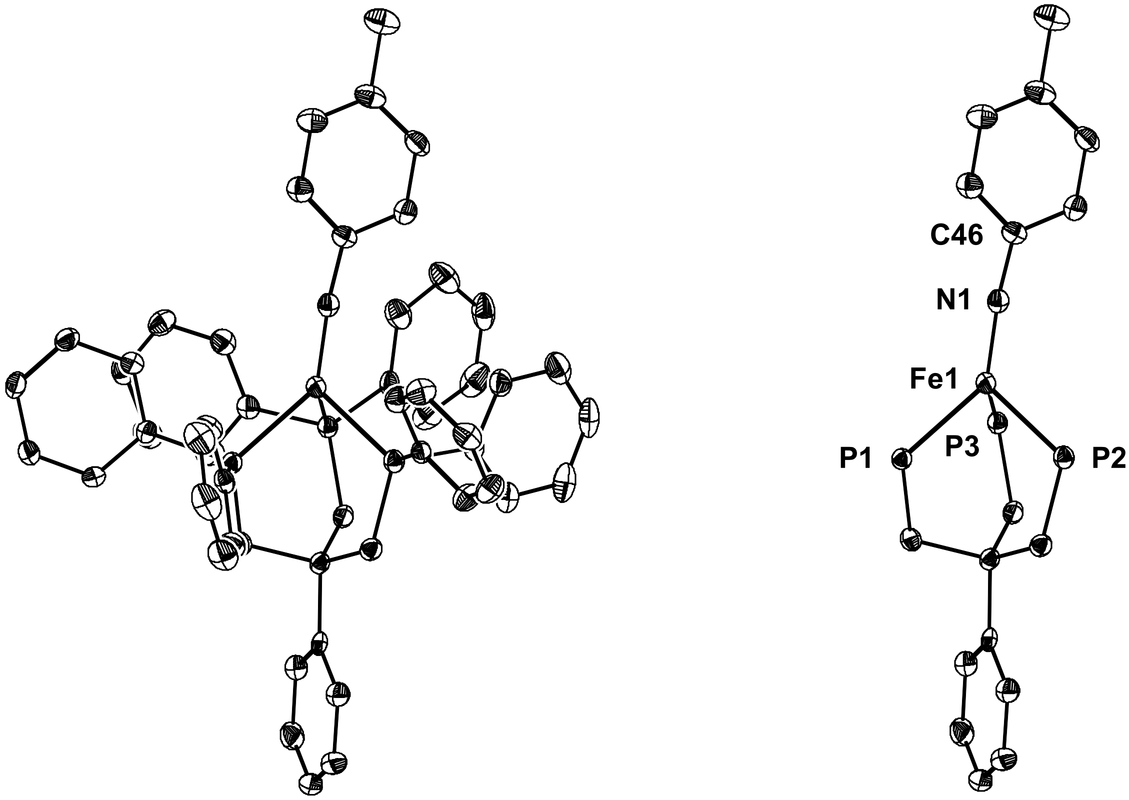

Figure 2.4. 50% thermal ellipsoid representation of $[PhBP_3]Fe{\equiv}N$-*p*-tolyl (**2.5**). For the image on the right, all phosphino phenyl groups have been removed for clarity. For both images, all hydrogen atoms and ½ of a benzene solvent molecule have been removed for clarity. Selected bond lengths (Å) and angles (°): Fe1-N1, 1.6578(19); N1-C46, 1.383(3); Fe1-P1, 2.2734(7); Fe1-P2, 2.2235(7); Fe1-P3, 2.2229(7); C46-N1-Fe1, 169.96(18); P1-Fe1-P2, 91.77(3); P1-Fe1-P3, 88.46(3); P2-Fe1-P3, 86.89(3); N1-Fe1-P1, 136.89(7); N1-Fe1-P2, 119.83(7); N1-Fe-P3, 119.38(7).

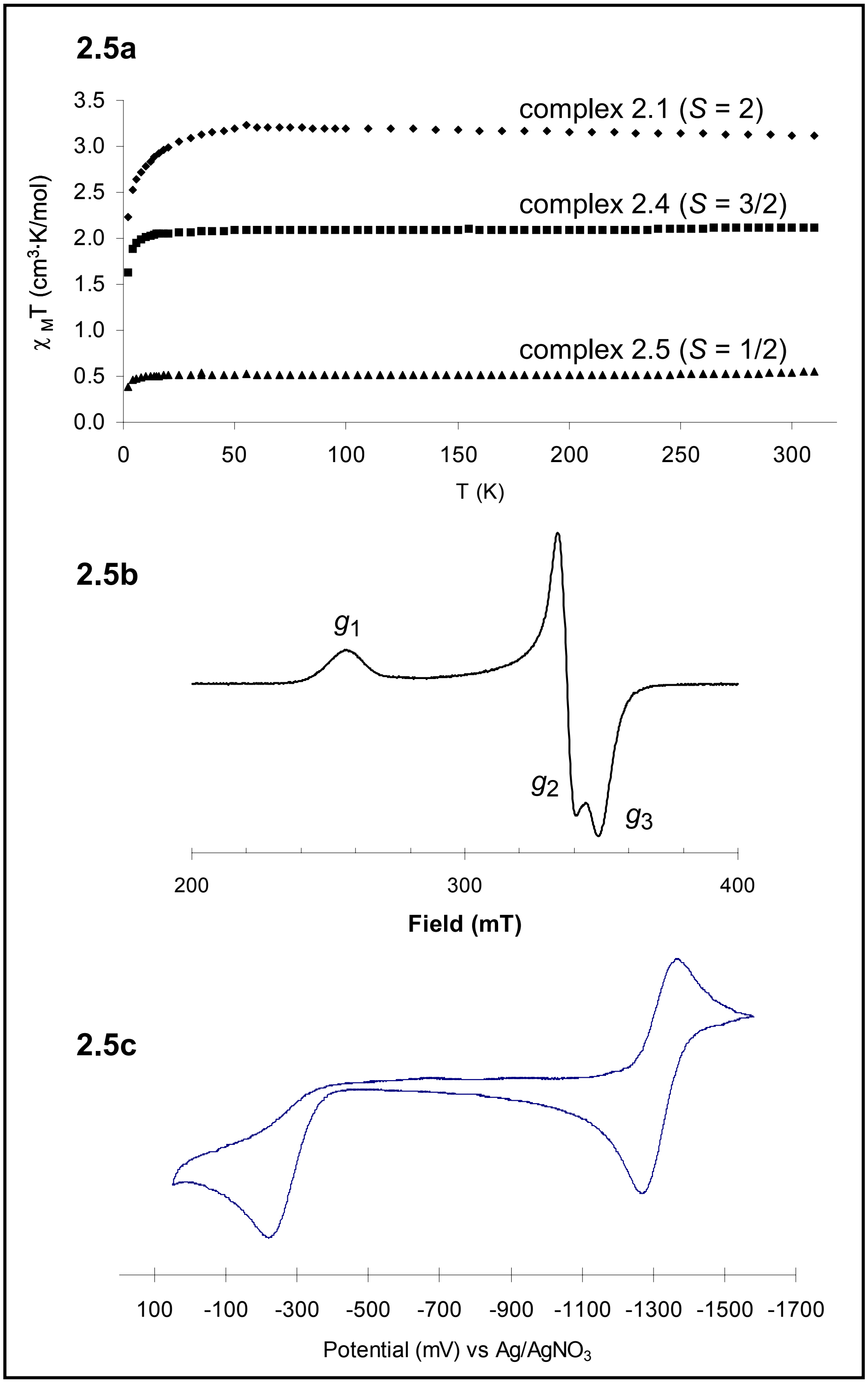

Figure 2.5. (a) SQUID magnetization data for complexes **2.1**, **2.4**, and **2.5**. (b) EPR spectrum of **2.5** (glassy toluene at 30 K, X-band, 9.474 GHz). (c) Cyclic voltammetry of **2.5** (THF, 0.3 M [TBA][PF_6], scan rate = 30 mV/s).

The rhombic EPR spectrum for **2.5** shows g_1 in the region 2.61, suggesting the unpaired spin resides in an orbital orthogonal to the Fe(1)-N(1) vector, and g_2 and g_3 in the region 2.0. While the three components g_1, g_2, and g_3 are well resolved at 30 K, g_2 and g_3 were not resolved at 77 K. Assignment of the electronic configuration of **2.5** can be made cautiously by assuming approximate three-fold symmetry and placing the molecular z-axis along the Fe-N bond vector. Using this coordinate system we suggest that a half-filled d_{xy} orbital sits slightly above two lower-lying and filled $d_{x^2-y^2}$ and d_{z^2} orbitals to provide the ground-state configuration $(d_{z^2})^2(d_{x^2-y^2})^2(d_{xy})^1(d_{xz})^0(d_{yz})^0$.[22] This electronic model suggests that it should be possible to reduce **2.5** by one electron, in accord with its cyclic voltammetry. A well-behaved and fully reversible $Fe^{II/III}$ couple is observed at -1.35 V, whereas an irreversible oxidation is observed at ~ -300 mV in the CV (Figure 2.5c). That **2.5** can be reversibly reduced to the d^6 anion "$\{[PhBP_3]Fe{\equiv}NAr\}^-$" is plausible, given the stability of its isolobal and isoelectronic d^6 relative $[PhBP_3]Co{\equiv}NAr$.[23] The chemical reduction of **2.5** by one electron occurs readily in the presence of a sodium/mercury amalgam to yield the anionic imide, $\{[PhBP_3]Fe{\equiv}N$-*p*-tolyl$\}\{Na(THF)_2\}$ (**2.6**), which was isolated in high-yield (88%) and features a singlet resonance at δ 87 ppm in its ^{31}P NMR spectrum. The difficulty in obtaining suitable crystals for X-ray diffraction analysis impeded a comparative structural study with **2.5**.[24]

As shown in Equation 2.3, the reaction between **2.4** and a variety of aryl- and alkyl-substituted organic azides may be utilized for the synthesis of a number of terminal Fe(III) imides. Curiously, however, no reaction was observed with trimethylsilyl azide despite the facile reactivity of **2.4** with *tert*-butylazide.[25] The phosphaimide byproducts

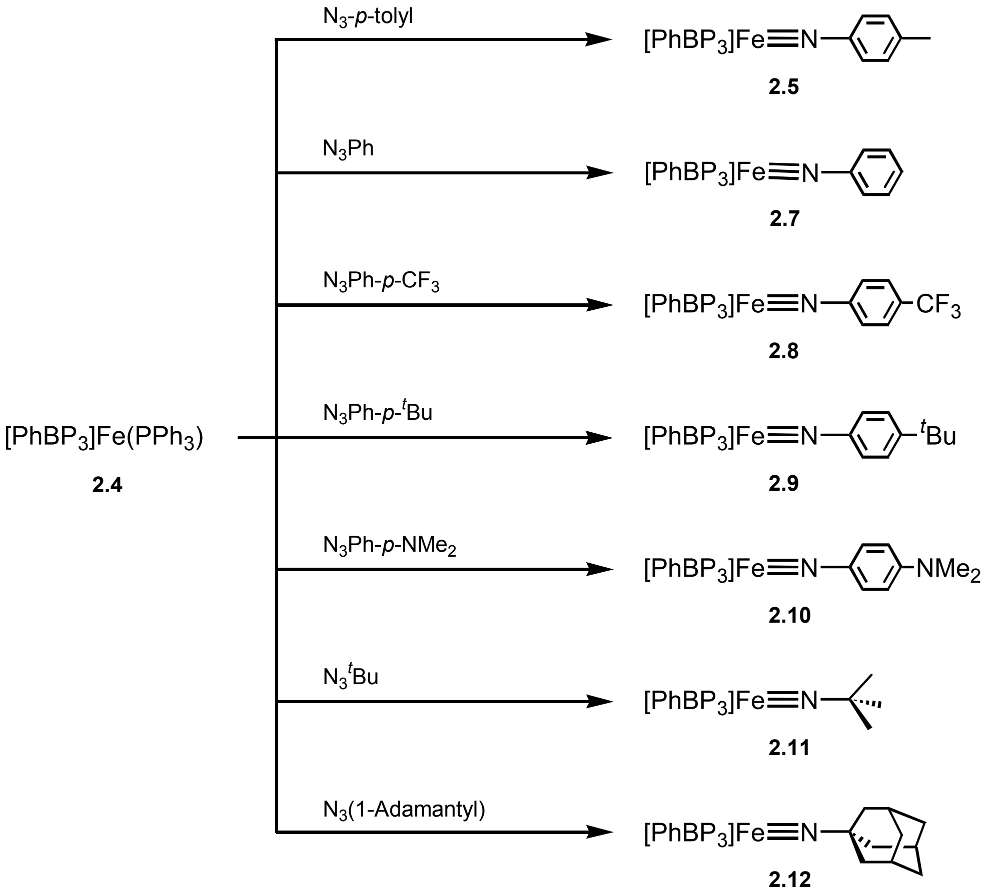

(2.3)

from these reactions may be removed by thorough washing with petroleum ether for compounds **2.8**, **2.11**, and **2.12**. For the remaining imides, purification by crystallization or precipitation from benzene solution with petroleum ether is required. All of the aryl imides are green in color and with the exception of **2.10**, feature absorptions in the UV-vis region that range from 630 to 638 nm with ε values from 2300 to 3400 cm^{-1} M^{-1}. Also present is a distinct shoulder at higher energy (~ 400 nm). These electronic transitions are presumably charge-transfer in nature, and the data obtained for aryl imides **2.5**–**2.10** are shown in Figure 2.6. Alkyl imides **2.11** (λ = 418, 506 nm; ε = 1300, 830 cm^{-1} M^{-1}) and **2.12** (λ = 422, 510 nm; ε = 1600, 1050 cm^{-1} M^{-1}) are brown in color and feature less intense absorptions than their aryl congeners.

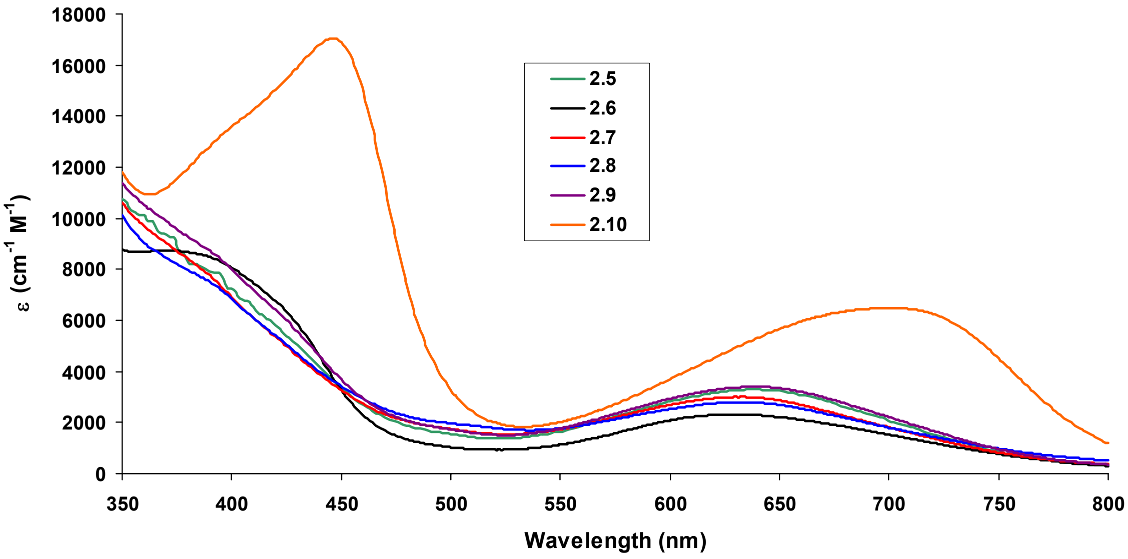

Figure 2.6. Uv-vis data for imides **2.5–2.10**.

Structural analysis of **2.11** (Figure 2.7) revealed a more C_3 symmetric structure than that observed for **2.5**. Nearly idealized *sp*-hybridization was observed for the imide nitrogen as evidenced from the Fe(1)-N(1)-C(46) bond angle of 179.17(13)° (for **2.5** Fe(1)-N(1)-C(46) = 169.96(18)°). Also present is a characteristically short iron-nitrogen linkage of 1.6346(13) Å, which is consistent with multiple bonding character. These structural parameters are very similar to those observed for $[PhB^{iPr}_3]Fe\equiv N(1\text{-}Ad)$ (Fe-N-C = 176.2(0)°, Fe-N = 1.638(2)), which is prepared from the addition of two equivalents of *tert*-butylazide to a solution of $\{[PhBP^{iPr}_3]Fe\}_2(\mu\text{-}N_2)$.[18] The increased symmetry of **2.11** is manifested in its axial EPR spectrum (Figure 2.8), in which the observed $g_\perp$ signal in the region 1.95 was not resolved even at temperatures as low as 5 K. Similar to the EPR data obtained for **2.5**, the $g_\parallel$ region at 2.91 suggests that the unpaired electron resides in an orbital orthogonal to the Fe-N vector.

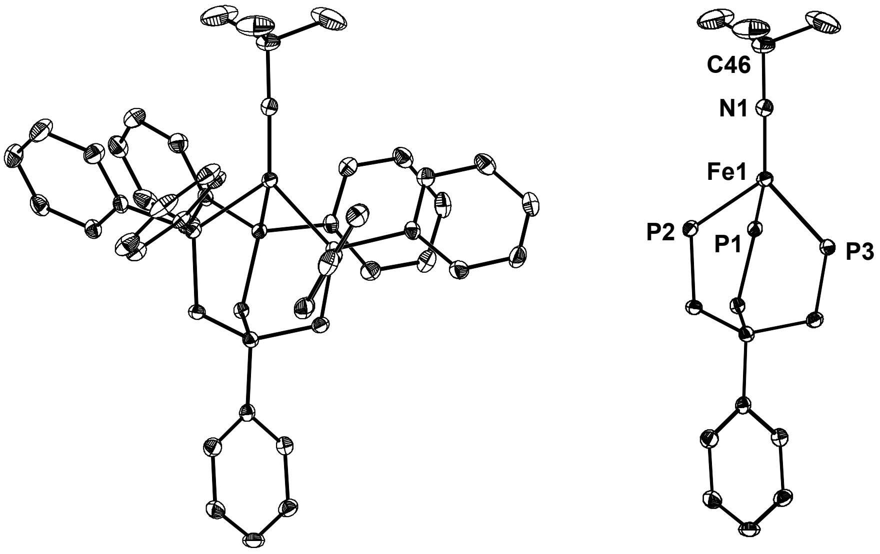

Figure 2.7. 50% thermal ellipsoid representation of [PhBP$_3$]Fe≡N^{t}Bu (**2.11**). For the image on the right, all phosphino phenyl groups have been removed for clarity. For both images, all hydrogen atoms have been removed for clarity. Selected bond lengths (Å) and angles (°): Fe1-N1, 1.6346(13); N1-C46, 1.442(2); Fe1-P1, 2.2427(5); Fe1-P2, 2.2153(5); Fe1-P3, 2.2531(5); C46-N1-Fe1, 179.17(13); P1-Fe1-P2, 89.96(2); P1-Fe1-P3, 91.16(2); P2-Fe1-P3, 89.38(2); N1-Fe1-P1, 125.80(5); N1-Fe1-P2, 117.83(5); N1-Fe-P3, 131.04(5).

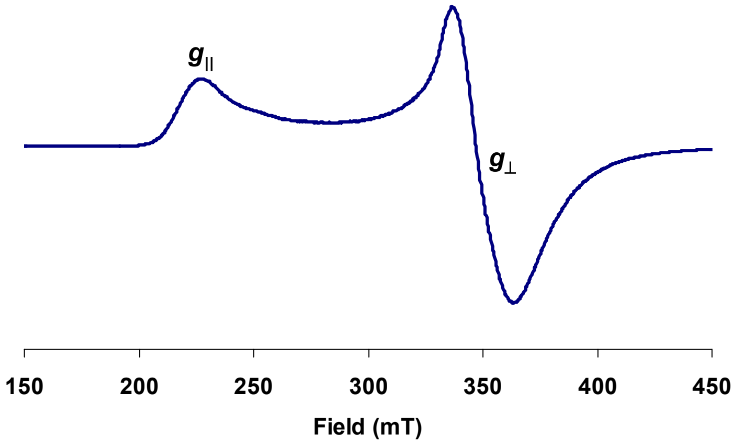

Figure 2.8. EPR spectrum of **2.11** (glassy toluene at 4 K, X-band, 9.378 GHz).

An electrochemical comparison between **2.5**, **2.11**, and **2.12** (Figure 2.9) demonstrates that more electron density is present at the metal center for the alkyl substituted imides, as evidenced by their more negative redox potentials for the $Fe^{II/III}$ couple ($E_{1/2}$ = -1206, -1350, and -1317 mV, respectively). The nature of the irreversible oxidative events at ~ -200 mV has not been rigorously established; possibilities include borate ligand oxidation or the formation of a cationic, high-valent Fe^{IV} species.

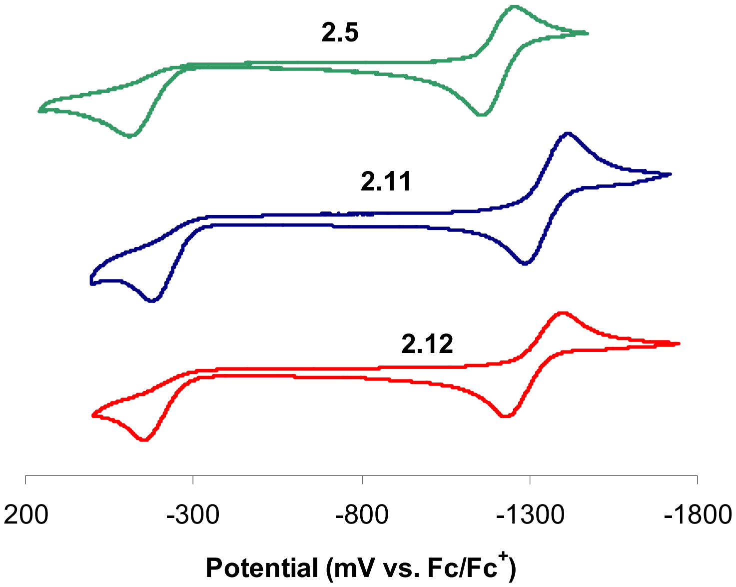

Figure 2.9. Cyclic voltammetry of **2.5**, **2.11**, and **2.12** (THF, 0.3 M [TBA][PF_6], scan rate = 30 mV/s for **2.5**, 100 mV/s for **2.11** and **2.12**).

2.2.4 Imide Synthesis via Metathesis

Although the iron(III) imides presented above are readily synthesized with an iron(I) precursor and organic azides, their synthesis using more conventional metathesis is of interest. For example, Bergman's family of d^6 iridium imides with the general formula $Cp^*Ir{\equiv}NR$ is generated upon reacting $[Cp^*IrCl_2]_2$ with four equivalents of [Li][N(H)R].[26] Lee generated his tetranuclear imide via the reaction of $FeCl_3$ with 2 equiv. of [Li][N(H)^{t}Bu][6c] while Hillhouse employed a deprotonation-oxidation strategy for the preparation of (dtbpe)Ni=NAr (dtbpe = 1,2 bis(di-*tert*-butylphosphino)ethane; Ar = 2,6-di-*iso*-propylphenyl).[27]

Two metathetic strategies may be envisioned for the preparation of [PhBP$_3$]Fe≡NR. As shown in Equation 2.4, the first involves the reaction of an iron(III) dihalide with two equivalents of a lithiated amide. This strategy has proven successful for the synthesis of [PhBP$_3$]Co≡NR complexes.[28] The second approach involves the reaction of iron(II) halides with lithiated amides, followed by deprotonation and oxidation.

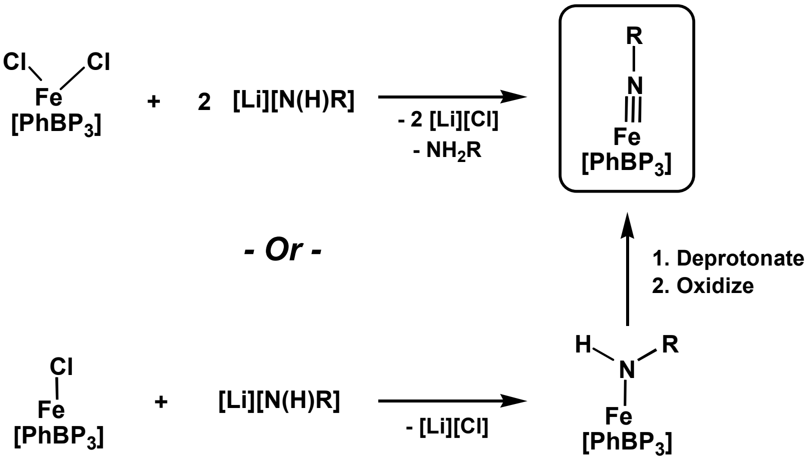

2.1

(2.4)

All attempts to synthesize an Fe(III) dihalide species have been unsuccessful. These include the oxidation of **2.1** in the presence of excess halide ions, or the metallation of FeBr$_3$ with [Tl][BP$_3$]. The lack of any isolable iron(III) product from these experiments is in agreement with the observed cyclic voltammetry of **2.1**, for which only a reversible Fe$^{II/I}$ couple was observed. However, **2.1** does react readily with a variety of lithiated amides to form the desired iron(II) amide. For example, the reaction between **2.1** and [Li][N(H)-*p*-tolyl] generates [PhBP$_3$]FeN(H)-*p*-tolyl, whose detailed synthetic protocol, characterization, and reactivity are presented in Chapter 3. Once purified, the deprotonation of $[PhBP_3]FeN(H)$-*p*-tolyl to yield $\{[PhBP_3]Fe{\equiv}N$-*p*-tolyl$\}^-$ readily occurs in the presence of a variety of bases, which was verified with ^{31}P NMR spectroscopy. Problematic with this synthetic route, however, is the absence of a high-yielding oxidative protocol. Varieties of ferrocinium salts, as well as the tropylium cation, have been canvassed to effect the oxidation of $\{[PhBP_3]Fe{\equiv}N$-*p*-tolyl$\}^-$, but yields of **2.5** were never greater than ~ 10% and separation of the desired Fe(III) product from the reaction matrix proved difficult.

2.2.5 Raman Characterization of the Fe≡NR Linkage

Multiply bonded iron-nitrogen species are proposed as key intermediates in a number of group-transfer processes,[29] including industrial nitrogen fixation,[30] and vibrational spectroscopy provides a means for their *in situ* detection. Therefore, providing a spectroscopic benchmark for low molecular weight $Fe-N_x$ linkages may prove essential to the analysis of potential intermediates during catalytic processes. Analysis of **2.5** with infrared spectroscopy did not reveal the presence of any vibration(s) that could unambiguously be assigned to the Fe≡NR linkage. Having established the presence of an intense chromophore with the aryl imides (*vida supra*), and to a lesser extent the alkyl imides, a collaboration with Prof. Larry Que and Dr. Mark Mehn of the University of Minnesota was initiated to examine their vibrational properties with resonance Raman spectroscopy.[31]

Initial studies with the iron(III) system focused on the evaluation of **2.7** and its isotopically labeled derivatives: **2.7**-^{15}N, **2.7**-(Ph-d_5), and **2.7**-(^{15}N, Ph-d_5). Excitation into the low-energy charge-transfer band of these complexes with 647.1 nm light affords a

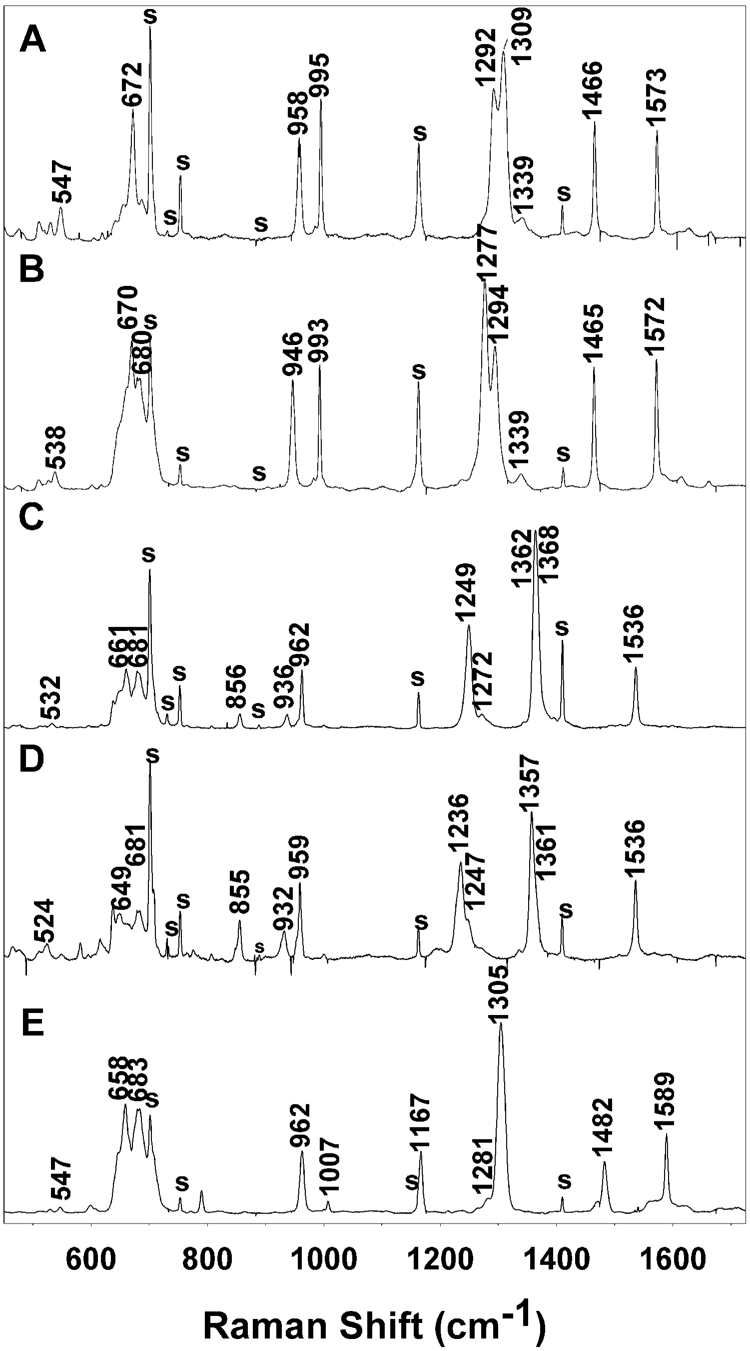

Figure 2.10. Resonance Raman spectra of (A) $[PhBP_3]Fe{\equiv}NPh$ (**2.7**), (B) $[PhBP_3]Fe{\equiv}^{15}NPh$ (**2.7**-^{15}N), (C) $[PhBP_3]Fe{\equiv}NPh$-d_5 (**2.7**-(Ph-d_5)), (D) $[PhBP_3]Fe{\equiv}^{15}NPh$-$d_5$ (**2.7**-(^{15}N, Ph-d_5)), and (E) $[PhBP_3]Fe{\equiv}N$-*p*-tolyl. All spectra were obtained at 77 K using a back-scattering geometry (647.1 nm excitation). Peaks due to solvent are marked with an ‘s’.

rich Raman spectrum in each case (Figure 2.10). For **2.7** (Figure 2.10A), several prominent non-solvent features are present. The vibrations at 958, 995, 1292, and 1309 cm^{-1} involve displacement of the nitrogen atom as a downshift in energy is observed upon ^{15}N substitution (**2.7**-(^{15}N); Figure 2.10B). The two modes with the greatest isotopic displacement, 958 → 946 cm^{-1} ($\Delta E = 12\ cm^{-1}$) and 1309 → 1277 cm^{-1} ($\Delta E = 32\ cm^{-1}$), are candidates for the Fe≡N vibration as shifts of 26 and 35 cm^{-1}, respectively, are expected from a diatomic harmonic oscillator model. The feature at 1309 cm^{-1} is also highly sensitive to deuteration of the aryl ring (**2.7**-(Ph-d_5); Figure 2.10C), suggesting that it is predominantly of N-Ar character. Therefore the vibration at 958 cm^{-1} is assigned to the Fe≡N linkage. The doubly labeled sample, **2.7**-(^{15}N, Ph-d_5) (Figure 2.10D), which is anticipated to decouple the Fe≡N and N-Ar modes, features a mode at 932 cm^{-1} which is the calculated value of 26 cm^{-1} lower in energy than that observed for the Fe≡N mode of naturally abundant **2.7**. Further support for the Fe≡N assignment is obtained through analysis of **2.5** (Figure 2.10E), which features a mode at 962 cm^{-1} that is assigned as $\nu_{Fe\equiv N}$.

In order to eliminate vibrational modes associated with the aromatic ring of **2.7**,[32] resonance Raman studies with alkyl imide **2.11**, **2.11**-d_9, and a 1:1 mixture of **2.11**:**2.11**-^{15}N were pursued.[33] As shown in Figure 2.11, the resulting data from excitation into the high-energy charge-transfer band with 406.7 nm light affords rich Raman spectra that, although less intense than those obtained for **2.7** and its labeled derivatives, are readily interpreted. Figure 2.11A features peaks at 1104 and 1233 cm^{-1} obtained for naturally abundant **2.11** that, upon analysis of a 1:1 mixture of **2.11**:**2.11**-^{15}N (Figure 2.11B), split into doublets as expected for the presence of equal amounts of ^{14}N and ^{15}N.

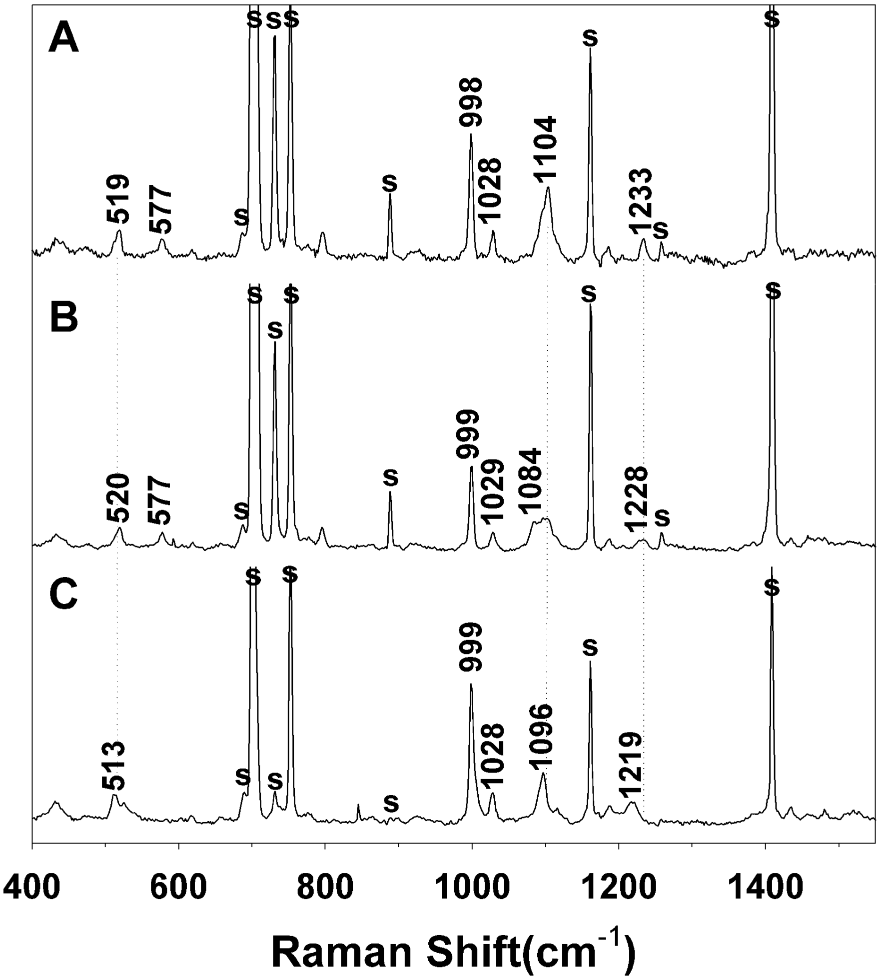

Figure 2.11. Resonance Raman spectra of (A) [PhBP$_3$]Fe≡N^{t}Bu (**2.11**), (B) 1:1 [PhBP$_3$]Fe≡N^{t}Bu : [PhBP$_3$]Fe≡^{15}N^{t}Bu (**2.11**:**2.11**-^{15}N), and (C) [PhBP$_3$]Fe≡N^{t}Bu-*d*$_9$. All spectra were obtained at 77 K using a back-scattering geometry (406.7 nm excitation). Peaks due to solvent are marked with an ‘s’.

The peak at 1104 cm^{-1} shifts to 1084 cm^{-1} (ΔE = 20 cm^{-1}), while the peak at 1233 cm^{-1} shifts to 1228 cm^{-1} (ΔE = 5 cm^{-1}). This demonstrates that admixed character of the Fe≡N and N-Alkyl modes is still present, but to a much weaker extent than in the aryl systems. A simple diatomic is expected to downshift 30 cm^{-1}; therefore the 1104 cm^{-1} mode must possess significant Fe≡N character. Consistent with this assignment is the spectra obtained with **2.11**-*d*$_9$ (Figure 2.11C), in which the 1104 cm^{-1} feature observed for naturally abundant **2.11** shifts to 1096 cm^{-1}(ΔE = 8 cm^{-1}), while the 1233 cm^{-1} feature shifts to 1219 cm^{-1} (ΔE = 14 cm^{-1}). Deuteration of the alkyl group has a greater influence on the energy of the latter mode, which is therefore assigned to the N-alkyl linkage. A summary of the vibrational data obtained for both the alkyl and aryl systems, in addition to a variety of other metal imido species, is presented in Table 2.1.

Table 2.1. Metal-imido vibrational data (Resonance Raman in CH_2Cl_2 unless otherwise noted).

Compound	$\nu_{M\text{-}NR}$ (cm^{-1})	$\nu_{MN\text{-}R}$ (cm^{-1})	Ref.
Iron N-Alkyls			
$[PhBP_3]Fe{\equiv}N^tBu$	1104	1233	
$[PhBP_3]Fe{\equiv}{}^{15}N^tBu$	1084	1228	
$[PhBP_3]Fe{\equiv}N^tBu\text{-}d_9$	1096	1219	
$[Fe_4(\mu_3\text{-}N^tBu)_4(N^tBu)Cl_3]$[a]	1111	1214	6c
Iron N-Aryls			
$[PhBP_3]Fe{\equiv}NPh$	958	1292	
$[PhBP_3]Fe{\equiv}{}^{15}NPh$	946	1277	
$[PhBP_3]Fe{\equiv}NPh\text{-}d_5$	936	1249	
$[PhBP_3]Fe{\equiv}{}^{15}NPh\text{-}d_5$	932	1236	
$[PhBP_3]Fe{\equiv}NTol$	962	1281	
Cobalt N-Alkyls			
$[PhBP_3]Co{\equiv}N^tBu$	1103	1238	31
$[PhBP_3]Co{\equiv}{}^{15}N^tBu$	1084		31
$[PhBP_3]Co{\equiv}N^tBu\text{-}d_9$	1100	1226	31
Cobalt N-Aryls			
$[PhBP_3]Co{\equiv}NPh$	956	1307	31
$[PhBP_3]Co{\equiv}{}^{15}NPh$	944	1295	31
$[PhBP_3]Co{\equiv}NPh\text{-}d_5$	934	1252	31
$[PhBP_3]Co{\equiv}{}^{15}NPh\text{-}d_5$	934	1242	31
$[PhBP_3]Co{\equiv}NTol$	959	1317	31
Vanadium N-Aryls[b]			
$Cp^*_2V{\equiv}NPh$	934	1330	34
$Cp^*_2V{\equiv}{}^{15}NPh$	923	1307	34

[a] IR data, KBr   [b] IR data, Nujol

2.2.6 Initial Reactivity Studies of the Fe≡NR Linkage

Preliminary reactivity studies with imide **2.5** highlight its reactive nature by comparison to its cobalt congener [PhBP$_3$]Co≡NAr, which required forcing conditions to release its "NAr" group to CO (70 °C, 12 days).[12] Complex **2.5** reacted immediately and quantitatively at room temperature upon CO addition to release isocyanate (O=C=N-*p*-tolyl, external integration standard) and form the golden dicarbonyl byproduct [PhBP$_3$]Fe(CO)$_2$ (**2.13**). Complex **2.13** (ν_{CO} = 1979, 1914 cm^{-1}, cf. [PhTp^{tBu}]Fe(CO)^{4} = 1907 cm^{-1}) has been structurally characterized as a distorted square pyramid (Figure 2.12) and independently generated by reaction of **2.4** with excess CO. In light of the recent nickel chemistry reported by Hillhouse and Mindiola,[35] well-defined examples of nitrene transfer to CO with release of isocyanate are now established for first-row systems including Fe(III), Co(III), and Ni(II).

Particular to the present system is that dicarbonyl **2.13** is itself a precursor to imide **2.5** (Equation 2.5). An NMR tube experiment demonstrated that the addition of 2 equivalents of *p*-tolyl azide to **2.13** slowly (rt, C$_6$D$_6$, 44 h) effected its conversion back to imide **2.5**, along with the release of free isocyanate (80%, external standard). The extended reaction times characteristic of this reaction (when compared with the formation of **2.5** from **2.4** and *p*-tolyl azide) likely reflect slow dissociation of CO from iron if proceeding through a dissociative mechanism, or the formation of an electronically unfavorable 19 e$^-$ intermediate if proceeding through an associative mechanism.

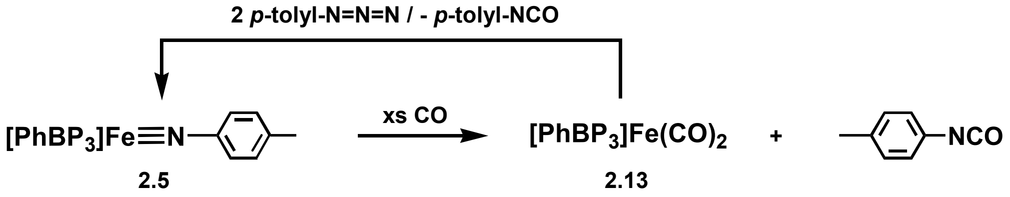

(2.5)

Despite these extended reaction times, catalytic isocyanate production is observed when a reaction vessel is cycled with azide and CO as necessary although conditions for an efficient "one-pot" catalytic procedure have yet to be established.

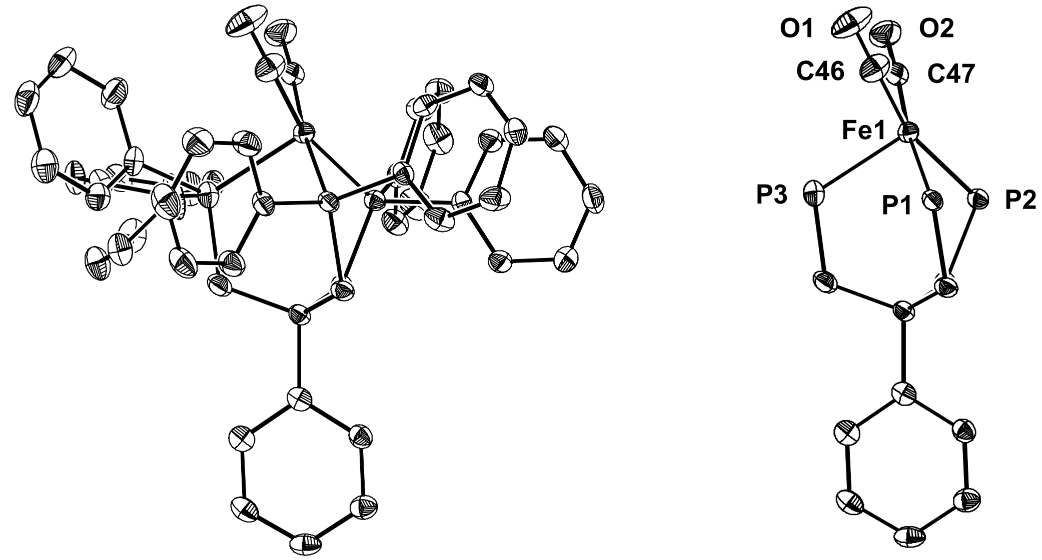

Figure 2.12. 50% thermal ellipsoid representation of [PhBP$_3$]Fe(CO)$_2$ (**2.13**). For the image on the right, all phosphino phenyl groups have been removed for clarity. For both images, all hydrogen atoms have been removed for clarity. Selected bond lengths (Å) and angles (°): Fe1-C46, 1.751(3); Fe1-C47, 1.768(3); Fe1-P1, 2.3103(8); Fe1-P2, 2.2819(8); Fe1-P3, 2.2626(8); C46-Fe1-P1, 92.83(10); C46-Fe1-P2, 164.62(10); C46-Fe1-P3, 99.50(10); C47-Fe1-P1, 173.88(9); C47-Fe1-P2, 92.67(9); C47-Fe1-P3, 96.35(9).

Although **2.5** does not react with acetonitrile at room temperature, group transfer chemistry is observed in the presence of isonitriles. Thus, exposure of **2.5** to excess ^{t}BuN≡C readily generates the five-coordinate iron(I) species, [PhBP$_3$]Fe(C≡N-^{t}Bu)$_2$ (**2.14**), with concomitant formation of the carbodiimide, ^{t}Bu-N=C=N-*p*-tolyl. As a final note concerning the reactivity of **2.5**, reaction conditions have yet to be established that facilitate aziridination chemistry. This behavior contrasts that of Hillhouse's d^8 Ni(II) system, which is capable of aziridinating ethylene upon gentle warming.[36]

2.3 Discussion

The preceding sections have presented structural, magnetic, and spectroscopic characterization for a number of 4-coordinate iron compounds supported by the first generation tris(phosphino)borate ligand, $[PhBP_3]$. Despite being coordinatively and electronically unsaturated, these complexes remain monomeric in the solid state and feature iron in the +1, +2, and +3 oxidation states while facilitating coordination chemistry with both π-acidic (CO) and π-basic (NR^{2-}) ligands. Compound **2.4** represents a rare example of 4-coordinate iron(I) that is readily oxidized by organic azides to yield terminal iron(III) imides.[37] The potential for these Fe≡NR linkages to engage in group transfer chemistry is highlighted in their reactivity to generate isocyanates and carbodiimides upon exposure to CO and isonitrile, respectively. These systems are inherently more reactive than their Co(III) congeners, which likely reflects the metalloradical character of the Fe(III) electronic configuration.

In contrast to the second generation "$[PhBP^{iPr}_3]$Fe" system, N_2 coordination was never observed with **2.1** under a variety of reductive conditions. This is attributed to the attenuated amount of electron density at the metal center for the parent $[PhBP_3]$ system, which is manifested in a comparative electrochemical study between the respective chloride derivatives. Such density is necessary for π-backbonding with N_2 and for stabilization of the B-C bonds with the ligand framework. Nevertheless, the steric and electronic properties of $[PhBP_3]$ that facilitate the formation of Fe≡NR linkages are topics of considerable interest. Recent studies in the Tilley lab with $[PhBP_3]$Ir, Cp^*Ir, and

[Tp^{Me2}]Ir complexes suggest that of these auxiliary ligands, [PhBP$_3$] is the most electron donating and sterically demanding.[38] The synergistic effect of these properties in engendering unique coordination environments was first realized with the isolation of an unprecedented, *low-spin* pseudotetrahedral cobalt(II) compound, [PhBP$_3$]CoI.[9]

As shown in Figure 2.13, this electronic anomaly is rationalized on the basis of an axial distortion (*i.e.*, L-M-L ~ 90° versus 109.5° for a tetrahedral system) that is enforced by the [PhBP$_3$] ligand, which results in a lowering of the a$_1$ orbital in C_{3v} symmetry. The extent to which this orbital is lowered, in combination with the destabilizing effect of the strong-field phosphine donors on the σ^* orbitals of the upper e set, determines whether it is energetically favorable to form a high-spin species or spin-pair the electrons to form a low-spin species. For [PhBP$_3$]CoI, the latter electronic situation is preferred and a Jahn-Teller elongation of one Co-P bond distance results from placing the seventh d-electron in the upper e set.[12] The inability of [Tp] ligands to stabilize a low-spin electronic

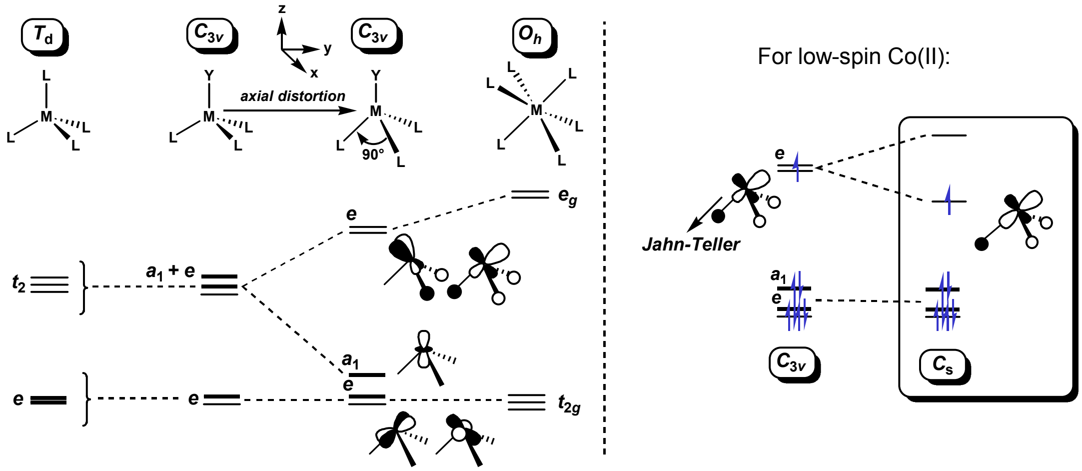

Figure 2.13. (*left*) Qualitative d-orbital splitting diagram illustrating the decent in symmetry from T_d to axially distorted C_{3v}. (*right*) Qualitative d-orbital splitting diagram illustrating the Jahn-Teller distortion observed for [PhBP$_3$]CoI. This figure is adapted from reference [12].

ground-state for pseudotetrahedral cobalt(II)[17c,39] likely arises from two factors: (1) the weaker field splitting effects of the nitrogenous ligands (*i.e.*, the upper e set that is σ^* with respect to the pyrazolyl donors is not as destabilized as it is with phosphine donors), and (2) the geometrical rigidity of the [Tp] framework, which may not be capable of accommodating a Jahn-Teller distortion.[40]

Although halides **2.1**–**2.3** feature high-spin electronic configurations, the preceding electronic arguments suggest that under C_3 symmetry, *low-spin* d_5 and d_6 iron species should be stable as the SOMO or HOMO, respectively, would be of relatively non-bonding character. One method for obtaining this low-spin configuration involves further destabilization of the upper e set through the installation of a π-basic ligand. This would make spin-pairing of the d-electrons energetically favorable when compared with placing them in relatively high-energy d-orbitals that now feature σ^* and π^* character. Such an electronic situation is in fact observed when NR^{2-} ligands are installed in the fourth coordination site of the "[$PhBP_3$]Fe" subunit.

The electronic structures of transition metal imido compounds have been discussed in some detail,[41] and the unique nature of the Fe≡NR linkages presented herein warrants further consideration of the d-orbital manifold. For Bergman's $Cp^*Ir{\equiv}NR$ systems,[26] the d_z^2 orbital is presumed to not interact too strongly with the Cp^* ligand, a common feature of metallocenes.[42] Consequently, the Ir-N σ-bond was largely attributed to interactions between the nitrogen σ-orbital and the Ir-p_z orbital (with some admixed d_z^2 character), rendering the d_z^2 orbital essentially non-bonding. Whether the d_z^2 orbital (with some admixed s and p_z character) actually lies lowest in energy for the [$PhBP_3$]Fe≡NR systems was of particular interest, and a DFT study with alkyl imide **2.11** was examined.

A restricted DFT geometry optimization calculation using the X-ray coordinates of **2.11** as the initial HF guess demonstrates several salient features concerning its electronic structure. As shown in Figure 2.14, the highest-lying metal-based orbitals are of d_{xz} and d_{yz} parantage and are π^* with respect to the imido nitrogen atom. This calculation is therefore consistent with solid-state data when ascribing triple bond character to the Fe≡NR linkage. Also evident is the relatively non-bonding nature of the orbital with d_{z^2} parentage, which is only slightly higher in energy than the filled orbital of non-bonding character in the xy plane (d_{xy} or $d_{x^2-y^2}$). The SOMO has been ordered as the lowest-lying orbital, which is likely a consequence of the restricted nature of the open-shell calculation and prevents the determination of a reliable SOMO-LUMO gap.[43]

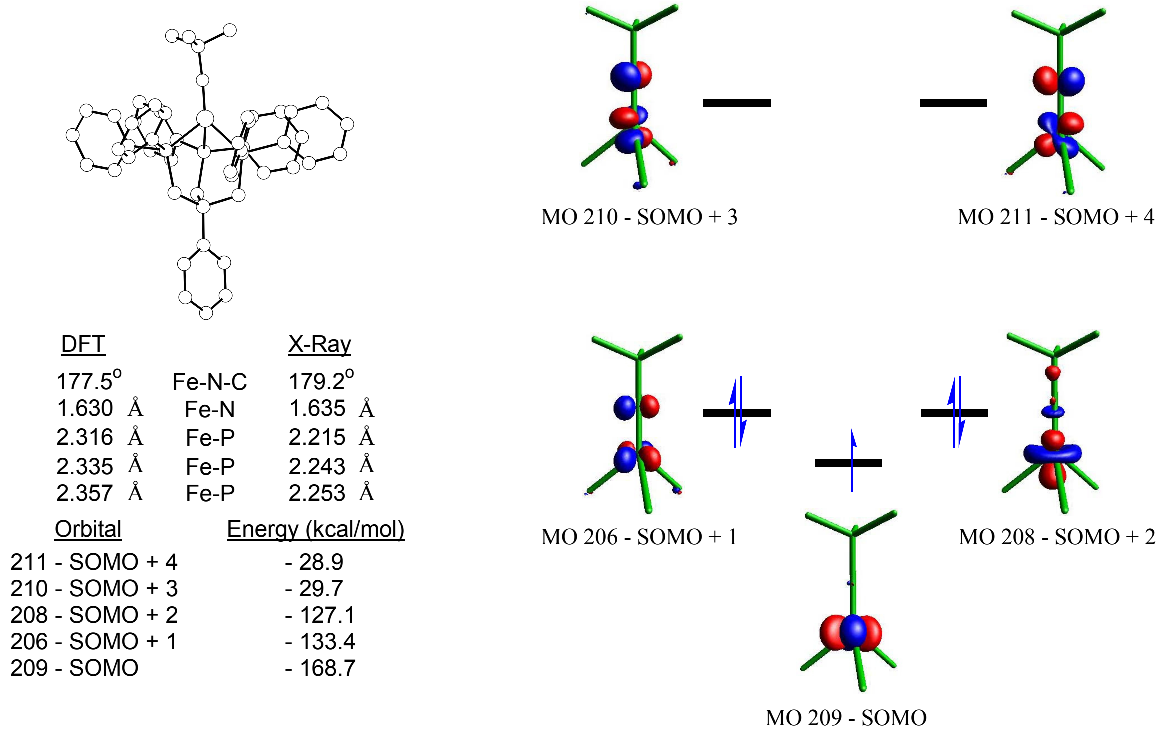

DFT		X-Ray
177.5°	Fe-N-C	179.2°
1.630 Å	Fe-N	1.635 Å
2.316 Å	Fe-P	2.215 Å
2.335 Å	Fe-P	2.243 Å
2.357 Å	Fe-P	2.253 Å

Orbital	Energy (kcal/mol)
211 - SOMO + 4	- 28.9
210 - SOMO + 3	- 29.7
208 - SOMO + 2	- 127.1
206 - SOMO + 1	- 133.4
209 - SOMO	- 168.7

Figure 2.14. Theoretically predicted geometry and electronic structure (DFT, JAGUAR 5.0, B3LYP/LACVP**) for S = ½ [PhBP$_3$]Fe≡N^{t}Bu (**2.11**). Structural parameters are highlighted within the figure.

The fact that the unpaired electron is calculated to reside in the xy plane is in agreement with the $g_{\parallel}$ values of 2.61 and 2.91 observed in the EPR spectra obtained for **2.5** and **2.11**, respectively, which demonstrate considerable angular momentum dependence.

These electronic considerations suggest that an isoelectronic oxo ligand (O^{2-}) should be compatible with the "[$PhBP_3$]Fe" platform to generate an iron(III) oxo, [$PhBP_3$]Fe(O). However, DFT studies with [$PhBP^{iPr}_3$]Fe≡N demonstrate that significant electronic changes are observed upon going from an M≡NR linkage to a terminal M≡N linkage.[44] In fact, two properties were noted that significantly destabilize the orbital of a_1 character in C_{3v} symmetry. The first concerns the L-Fe-L angles, which are appreciably expanded (99–101°) to yield a structure more tetrahedral in nature. Additionally, the hybridization of the terminal atom allows for increased σ interactions with the a_1 orbital, resulting in significant σ^* character (a HOMO-LUMO gap of 3.90 eV is calculated for [$PhBP^{iPr}_3$]Fe≡N). As shown in Figure 2.15, an iron(III) system would place one electron in the now destabilized a_1 orbital, which is anticipated to yield a highly reactive and/or unstable linkage. A cationic iron(IV) oxo[45] would alleviate this situation, although this is an oxidation state that has yet to be observed with the [$PhBP_3$]Fe system.

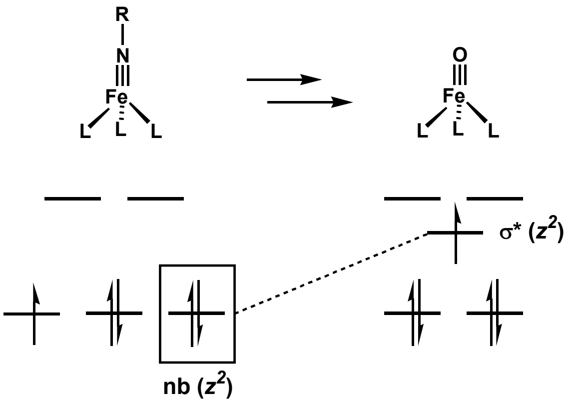

Figure 2.15. Qualitative d-orbital splitting diagram for a d^5 imide and a hypothetical d^5 oxo.

Resonance Raman experiments with **2.7** and its isotopically labeled derivatives provide a preliminary assignment of 958 cm^{-1} for the Fe≡N vibration (Figure 2.10) and demonstrate that the charge transfer band observed at ~ 640 nm (see Figure 2.6) in the UV-vis spectrum is associated with the Fe≡N linkage. This value is higher in energy than that of 876 cm^{-1} reported by Nakamoto for (TPP)Fe^{V}(N), although Nakamoto's value likely reflects attenuation of the Fe-N bond order resulting from occupation of the Fe-N π^* orbitals by two electrons.[46] The structurally related iron(IV) nitride, $[PhBP^{iPr}_3]Fe{\equiv}N$, features an Fe≡N vibration at 1034 cm^{-1}.[44] However, direct comparisons between the imide and nitride systems may not be warranted as the current study demonstrates that a significant degree of vibronic coupling exists between the Fe≡N and N-Ar vibrational modes (Figures 2.10 B, C, and D). A similar situation was reported for $Cp^*_2V{\equiv}NPh$,[34] in addition to Lee's tetranuclear iron imide ($\nu_{Fe\equiv N}$ = 1111 cm^{-1}).[6c] Thus for the imides under investigation, a pure Fe≡N vibration is not observed and the experimental value may actually reflect an average of the symmetric and anti-symmetric stretches of the Fe≡N-Ar linkage.[47] Resonance Raman experiments with the $[PhBP_3]$Co(III) aryl imide systems (see Table 2.1) are similar in that extensive coupling between the Co≡N and N-Ar linkages is observed.

Resonance Raman data obtained for **2.11** and its isotopically labeled derivatives are significantly easier to interpret than those obtained for the aryl system (Figure 2.11). This is presumably due to the absence of any aryl vibrational modes, and from these data a value of 1104 cm^{-1} is proposed for $\nu_{Fe\equiv N}$. As alluded to above, direct comparisons with terminal systems are tenuous at best, as a pure Fe≡N vibration is not observed due to vibronic coupling between the Fe≡N and N-^{t}Bu linkage.

2.4 Conclusions

In summary, this work shows that Fe(I) supported by a strong field and tripodal phosphine donor can undergo a facile, multielectron group transfer process to accept a strongly π-donating imide ligand. The imide can be subsequently released to the acceptor substrate CO. The method of formation of imide **2.5**, its reactivity with CO, and its regeneration from **2.13** underscore the viability of a well-defined, Fe(I) → Fe(III)/Fe(III) → Fe(I) group transfer loop. Whether parallels to such group transfer processes occur in biological systems, such as the reducing FeS-clusters of certain metalloenzymes, is worth considering.

2.5 Experimental Section

2.5.1 General Considerations

All manipulations were carried out using standard Schlenk or glove-box techniques under a dinitrogen atmosphere. Unless otherwise noted, solvents were deoxygenated and dried by thorough sparging with N_2 gas followed by passage through an activated alumina column. Non-halogenated solvents were tested with a standard purple solution of sodium benzophenone ketyl in tetrahydrofuran in order to confirm effective oxygen and moisture removal. Elemental analyses were performed by Desert Analytics, Tucson, AZ. Deuterated benzene was purchased from Cambridge Isotope Laboratories, Inc. and was degassed and dried over activated 3 Å molecular sieves prior to use. A Varian Mercury-300 NMR spectrometer was used to record ^{1}H, ^{31}P, and ^{19}F NMR spectra at ambient temperature. ^{1}H chemical shifts were referenced to residual solvent. ^{31}P chemical shifts were referenced to 85% H_3PO_4 at δ 0 ppm, and ^{19}F chemical shifts were referenced to C_6F_6 at δ -167.7 ppm. MS data for samples were obtained by injecting a benzene solution into a Hewlett-Packard 1100MSD mass spectrometer equipped with an electrospray (ES) ionization chamber. UV-vis measurements were taken on a Hewlett Packard 8452A Diode Array Spectrometer using a quartz cell with a Teflon cap. IR measurements were obtained with a KBr solution cell using a Bio-Rad Excalibur FTS 3000 spectrometer controlled by Bio-Rad Merlin Software (v. 2.97) set at 4 cm^{-1} resolution.

2.5.2 Magnetic Measurements

Measurements were recorded using a Quantum Designs SQUID magnetometer running MPMSR2 software (Magnetic Property Measurement System Revision 2). Data were recorded at 5000 G. Samples were suspended in the magnetometer in a clear plastic straw sealed under nitrogen with Lilly No. 4 gel caps. Loaded samples were centered within the magnetometer using the DC centering scan at 35 K and 5000 G. Data were acquired at 2–10 K (one data point every 2 K), 10–60 K (one data point every 5 K), and 60–310 K (one data point every 10 K). The magnetic susceptibility was adjusted for diamagnetic contributions using the constitutive corrections of Pascal's constants. The molar magnetic susceptibility (χ_m) was calculated by converting the calculated magnetic susceptibility (χ) obtained from the magnetometer to a molar susceptibility (using the multiplication factor {(molecular weight)/[(sample weight)*(field strength)]}). Curie-Weiss behavior was verified by a plot of χ_m^{-1} versus T. Effective magnetic moments were calculated using Equation 2.6. Solution magnetic moments were measured using Evans method.[10]

$$\mu_{eff} = \mathrm{sqrt}(7.997\ \chi_m T) \quad (2.6)$$

2.5.3 EPR Measurements

X-band EPR spectra were obtained on a Bruker EMX spectrometer (controlled by Bruker Win EPR Software v. 3.0) equipped with a rectangular cavity working in the TE_{102} mode. Variable temperature measurements were conducted with an Oxford continuous-flow helium cryostat (temperature range 3.6–300 K). Accurate frequency values were provided by a frequency counter built into the microwave bridge. Solution spectra were acquired in toluene. Sample preparation was performed under a dinitrogen atmosphere in an EPR tube equipped with a ground glass joint.

2.5.4 Electrochemical Measurements

Electrochemical measurements were carried out in a glove-box under a dinitrogen atmosphere in a one-compartment cell using a BAS model 100/W electrochemical analyzer. A glassy carbon electrode and platinum wire were used as the working and auxiliary electrodes, respectively. The reference electrode was $Ag/AgNO_3$ in THF. Solutions (THF) of electrolyte (0.3 M tetra-*n*-butylammonium hexafluorophosphate) and analyte (2 μM) were also prepared in a glove-box.

2.5.5 DFT Calculations

A hybrid density functional calculation was performed for **2.11** using the Jaguar package (version 5.0, release 20).[48] The calculation employed B3LYP with LACVP** (LACVP**$^{++}$ for B) as the basis set.[49] A geometry optimization was carried out using the X-ray coordinates for **2.11** as the initial HF guess. No symmetry constraints were imposed, and the calculation was performed assuming a doublet electronic ground state. Pictorial representations of the resulting molecular orbitals were generated using the gOpenMol software program.

2.5.6 Raman Measurements

Resonance Raman spectra were collected on an Acton AM-506 spectrometer (1200 groove grating) using a Kaiser Optical holographic super-notch filter with a Princeton Instruments liquid N_2 cooled (LN-1100PB) CCD detector with a 4 cm^{-1} spectral resolution. The laser excitation lines were obtained with a Spectra Physics 2030-KR-V krypton laser. The Raman frequencies were referenced to indene, and the entire spectral range was obtained by collecting spectra at several different frequency windows and splicing the spectra together. The spectra were obtained at 77 K using a back-scattering geometry on samples frozen on a gold-plated copper cold finger in thermal contact with a Dewar containing liquid N_2. Typical accumulation times were 16–32 minutes per frequency window. Curve fits (Gaussian functions) and baseline corrections (polynomial fits) were carried out using Grams/32 Spectral Notebase Version 4.04 (Galactic).

2.5.7 Starting Materials and Reagents

All reagents were purchased from commercial vendors and used without further purification unless otherwise noted. [Tl][PhBP_3],[9] *p*-tolylazide,[50] phenylazide,[50] N_3(Ph-*p*-CF_3),[51] N_3(Ph-*p*-NMe_2),[52] and *tert*-butylazide[53] were prepared according to literature procedures. N_3(Ph-*p*-^{t}Bu) was prepared following the procedure outlined for *p*-tolylazide but with 4-*tert*-butylaniline. [Na][^{15}NNN] was obtained from Cambridge Isotope Labs and used as received for the synthesis of *tert*-butylazide-^{15}N. The ^{15}N label resides in a 50:50 statistical distribution at the α and γ positions of the organic azide, resulting in 50% incorporation of the ^{15}N label into the corresponding metal imide when synthesized via azide decomposition. *tert*-butanol-d_9 was obtained from Cambridge and used as received for the synthesis of *tert*-butylazide-d_9. For Ph-^{15}NNN and d_5-PhN$_3$, aniline-^{15}N and aniline-2,3,4,5,6-d_5 were obtained from Aldrich and used as received. The doubly labeled azide, d_5-Ph-α-^{15}NNN, was synthesized from d_5-Ph-^{15}NH$_2$ which was prepared from the nitration of benzene-d_6 (Cambridge) with [NH$_4$][^{15}NO$_3$] (Cambridge)[54] followed by reduction with H$_2$ in the presence of 10 % Pd/C.

2.5.8 Synthesis of Compounds

Synthesis of [PhBP$_3$]FeCl, 2.1: FeCl$_2$ (0.285 g, 2.25 mmol) was added to THF (80 mL) with stirring. A THF slurry (40 mL) of [Tl][PhBP$_3$] (2.00 g, 2.25 mmol) was then added dropwise. During the addition, the reaction yellowed as TlCl precipitated from solution. After stirring overnight at room temperature, volatiles were removed under reduced pressure, and the crude solids were extracted with benzene (~ 30 mL). The benzene extract was then filtered over celite. Removal of the solvent under reduced pressure followed by washing with petroleum ether (3 x 30 mL) and drying afforded **2.1** as a yellow powder (1.45 g, 83 %). X-ray quality crystals were grown via vapor diffusion of petroleum ether into a benzene solution. ^{1}H NMR (C$_6$D$_6$, 300 MHz): δ 40.8 (s); 19.8 (s); 18.3 (s); 7.01 (s); -12.2 (s); -37.7 (br, s). UV-vis (C$_6$H$_6$) λ_{max}, nm (ε, M^{-1} cm^{-1}): 416 (580). SQUID (solid, average 10 – 310 K): $\mu_{eff} = 4.95\ \mu_B$. Evans Method (C$_6$D$_6$): 5.04 B.M. ES-MS: calcd. for C$_{45}$H$_{41}$BClFeP$_3$ (M)$^+$ 777 m/z, found (M – Cl)$^+$ 741 m/z. Anal. Calcd. for C$_{45}$H$_{41}$BClFeP$_3$: C, 69.57; H, 5.32. Found: C, 69.69; H, 5.21.

Synthesis of [PhBP$_3$]FeBr, 2.2: FeBr$_2$ (0.0240 g, 0.112 mmol) was added to THF (3 mL) with stirring. A THF slurry (3 mL) of [Tl][PhBP$_3$] (0.100 g, 0.112 mmol) was then added dropwise. During the addition, the reaction changed from brown to yellow as TlBr precipitated from solution. After stirring overnight, volatiles were removed under reduced pressure, and the crude solids were extracted with benzene (3 mL), filtered over Celite, lyophilized, and washed with petroleum ether (3 x 5 mL). The resulting yellow powder was dried to yield **2.2** (0.0775 g, 84 %). ^{1}H NMR (C_6D_6, 300 MHz): δ 37.0 (s); 18.2 (s); 17.1 (s); 8.89 (s); -11.2 (s); -32.9 (br, s). UV-vis (C_6H_6) λ_{max}, nm (ε, M^{-1} cm^{-1}): 424 (620). Evans Method (C_6D_6): 5.20 μ_B. ES-MS: calcd. for $C_{45}H_{41}BBrFeP_3$ $(M)^+$ 821 m/z, found $(M - Br)^+$ 741 m/z. Anal. Calcd. for $C_{45}H_{41}BBrFeP_3$: C, 65.81; H, 5.03. Found: C, 65.42; H, 4.87.

Synthesis of [PhBP$_3$]FeI, 2.3: FeI_2 (0.100 g, 0.323 mmol) was added to a THF/Et_2O solution (3 mL/3 mL) with stirring. A THF slurry (3 mL) of [Tl][PhBP$_3$] (0.287 g, 0.323 mmol) was then added dropwise. During the addition, the reaction gradually changed from purple to yellow as TlI precipitated from solution. After stirring overnight, volatiles were removed under reduced pressure, and the crude solids were extracted with benzene (5 mL), filtered over Celite, lyophilized, and washed with petroleum ether (3 x 5 mL). The resulting yellow powder was dried to yield **2.3** (0.237 g, 85 %). ^{1}H NMR (C_6D_6, 300 MHz): δ 29.4 (s); 15.1 (s); 14.6 (s); 12.1 (s); -8.96 (s); -22.9 (br, s). UV-vis (C_6H_6) λ_{max}, nm (ε, M^{-1} cm^{-1}): 438 (650). Evans Method (C_6D_6): 5.03 μ_B. ES-MS: calcd. for $C_{45}H_{41}BIFeP_3$ $(M)^+$ 868 m/z, found $(M - I)^+$ 741 m/z. Anal. Calcd. for $C_{45}H_{41}BIFeP_3$: C, 62.25; H, 4.76. Found: C, 62.60; H, 4.72.

Synthesis of [PhBP$_3$]Fe(PPh$_3$), 2.4: A 0.19 weight % Na/Hg amalgam (0.0296 g, 1.29 mmol of sodium dissolved in 15.6 g of mercury) was stirred in THF (50 mL). To this was added dropwise a THF solution (20 mL) of **2.1** (1.00 g, 1.29 mmol) and PPh_3 (1.01 g, 3.86 mmol). During the addition, the reaction changed from yellow to orange and finally a brown color approximately 20 minutes after the addition was complete.

After 15 hours, the reaction solution was decanted from the mercury, and volatiles were removed under reduced pressure. The crude solids were extracted with benzene (50 mL) and filtered over Celite. The filtrate was then concentrated under reduced pressure to approximately 20 mL, at which point a small amount of precipitate was evident. The addition of petroleum ether (150 mL) resulted in the precipitation of orange solids, which were collected on a sintered glass frit and washed with petroleum ether (3 x 15 mL). After drying, **2.4** was obtained as an orange powder (0.795 g, 62 %). X-ray quality crystals were grown via vapor diffusion of petroleum ether into a benzene solution. ^{1}H NMR (C_6D_6, 300 MHz): δ 13.1 (br, s); 11.1 (br, s); 8.51 (s); 7.49 (s); -1.09 (br, s); -2.68 (br, s). Evans Method (C_6D_6): 3.88 B.M. SQUID (solid, average 10 – 310 K): μ_{eff} = 4.09 μ_{B}. ES-MS: calcd. for $C_{63}H_{56}BFeP_4$ $(M)^+$ 1004 m/z, found $(M - PPh_3)^+$ 741 m/z. Anal. Calcd. for $C_{63}H_{56}BFeP_4$: C, 75.39; H, 5.62. Found: C, 75.60; H, 5.61.

Synthesis of [PhBP$_3$]Fe≡N-*p*-tolyl, 2.5: Compound **2.4** (0.600 g, 0.598 mmol) was dissolved in benzene (15 mL) with stirring. A benzene solution (2 mL) of *p*-tolylazide (0.159 g, 1.19 mmol) was added dropwise, during which time the reaction changed color from orange to an intense forest green. After 12 hours, volatiles were removed under reduced pressure, and the solids were washed with petroleum ether (3 x 20 mL) and collected on a sintered glass frit. Drying yielded 0.453 g of a forest green powder contaminated with the $Ph_3P=N$(*p*-tolyl) by-product. Crystallization from petroleum ether into benzene yielded pure **2.5** (0.255 g, 50 %). Alternatively, the benzene reaction solution may be concentrated to ~ 1/3 the volume and with the slow addition of petroleum ether, **2.5** selectively precipitates. The purity of **2.5** obtained from this method is dependent on the benzene/petroleum ether ratio. With the appropriate combination, pure **2.5** may be obtained. ^{1}H NMR (C_6D_6, 300 MHz): δ 26.4 (br, s); 13.8 (s); 13.3 (s); 10.4 (br, s); 9.90 (t, *J* = 6.6 Hz); 9.08 (t, *J* = 6.9 Hz); 7.93 (br, s); 5.47 (d, *J* = 6.6 Hz); 3.14 (s); -0.75 (s). UV-vis (C_6H_6) λ_{max}, nm (ε, M^{-1} cm^{-1}): 640 (3300). SQUID (solid, average 10 – 310 K): μ_{eff} = 2.03 μ_B. Evans Method (C_6D_6): 1.85 μ_B. Anal. Calcd. for $C_{52}H_{48}BFeNP_3$: C, 73.78; H, 5.72; N, 1.65. Found: C, 73.62; H, 5.84; N, 1.93.

Synthesis of {[PhBP$_3$]Fe≡N-*p*-tolyl}{Na(THF$_2$)}, 2.6: Imide **2.5** was stirred in THF (~5 mL) with a 0.19 weight % Na/Hg amalgam. After 4 hours the THF was decanted from the amalgam, and volatiles were removed under reduced pressure. The crude solids were washed with petroleum ether (10 mL) and dried to obtain **2.6** as a green solid (0.105 g, 88 %). ^{1}H NMR (C_6D_6, 300 MHz): δ 8.21 (d, *J* = 7.2 Hz, 2H); 7.89 (s, 12 H); 7.69 (m, 4H); 7.42 (t, J = 7.2 Hz, 1H); 6.90 (d, *J* = 8.4 Hz, 2H); 6.80 (m, 18H); 3.14 (m, 8H); 2.03 (s, 3H); 1.56 (s, 6H); 1.23 (m, 8H). ^{31}P{^{1}H} NMR (C_6D_6, 121.4 MHz): δ 87 (s). UV-vis (C_6H_6) λ_{max}, nm (ε, M^{-1} cm^{-1}): 630 (2300), 370 (8700). Anal. Calcd. for $C_{60}H_{64}BFeNNaO_2P_3$: C, 71.09; H, 6.36; N, 1.38. Found: C, 70.70; H, 6.13; N, 1.36.

Synthesis of [PhBP$_3$]Fe≡NPh, 2.7: Compound **2.4** (0.200 g, 0.199 mmol) was added to benzene (~5 mL) with stirring. A benzene solution (1 mL) of phenyl azide (0.0475 g, 0.399 mmol) was added dropwise, resulting in a rapid color change from orange to forest green. After 12 hours the reaction was concentrated to a volume of 2 mL under reduced pressure. The addition of petroleum ether (~18 mL) and stirring for an additional 30 minutes resulted in the precipitation of green solids, which were isolated on a medium porosity sintered glass frit. After washing with additional petroleum ether (3 x 10 mL), the green solids were dried under reduced pressure to yield **2.7** as a pure compound (0.119 g, 72 %). Crystals of **2.7** were grown via vapor diffusion of petroleum ether into a benzene solution. ^{1}H NMR (C_6D_6, 300 MHz): δ 14.0 (s); 13.3 (s); 10.1 (br, s); 9.90 (t, *J* = 6.0 Hz); 9.42 (br, s); 9.09 (t, *J* = 7.5 Hz); 5.37 (d, *J* = 7.5 Hz); 3.21 (t, *J* = 6.0 Hz); -0.65 (br, s); -7.19 (s). UV-vis (C_6H_6) λ, nm (ε, M^{-1} cm^{-1}): 632 (3000). Evans Method (C_6D_6): 1.87 μ_B. Anal. Calcd. for $C_{51}H_{46}BFeNP_3$: C, 73.58; H, 5.57; N, 1.68. Found: C, 73.73; H, 5.68; N, 1.76.

Synthesis of [PhBP$_3$]Fe≡N(Ph-*p*-CF$_3$), 2.8: Compound **2.4** (0.200 g, 0.199 mmol) was added to benzene (~5 mL) with stirring. A benzene solution (1 mL) of N_3(Ph-*p*-CF_3) (0.0475 g, 0.399 mmol) was then added dropwise, resulting in a rapid color change from orange to forest green. After 12 hours the reaction was concentrated to a volume of 2 mL under reduced pressure. The addition of petroleum ether (~18 mL) and stirring for an additional 30 minutes resulted in the precipitation of green solids, which were isolated on a medium porosity sintered glass frit. After washing with additional petroleum ether (3 x 10 mL), the green solids were dried under reduced pressure to yield **2.8** as a pure compound (0.123 g, 69 %). Crystals of **2.8** were grown via vapor diffusion of petroleum ether into a benzene solution. ^{1}H NMR (C_6D_6, 300 MHz): δ 14.8 (s); 13.2 (s); 9.86 (t, *J* = 6.0 Hz); 9.06 (t, *J* = 6.3 Hz); 8.71 (br, s); 8.54 (br, s); 5.21 (d, *J* = 6.3 Hz); 3.44 (t, *J* = 6.0 Hz); -0.41 (br, s). ^{19}F NMR (C_6D_6, 282 MHz): δ -27.2 (s). UV-vis (C_6H_6) λ, nm (ε, M^{-1} cm^{-1}): 632 (2800). Evans Method (C_6D_6): 1.80 μ_B. Anal. Calcd. for $C_{52}H_{45}BF_3FeNP_3$: C, 69.36; H, 5.04; N, 1.56. Found: C, 68.99.; H, 5.36; N, 1.70.

Synthesis of [PhBP$_3$]Fe≡N(Ph-*p*-^{t}Bu), 2.9: Compound **2.4** (0.200 g, 0.199 mmol) was added to benzene (~5 mL) with stirring. A benzene solution (1 mL) of N_3(Ph-*p*-^{t}Bu) (0.0698 g, 0.399 mmol) was added dropwise, resulting in a rapid color change from orange to forest green. After 12 hours the reaction was concentrated to a volume of 2 mL under reduced pressure. The addition of petroleum ether (~18 mL) and stirring for an additional 30 minutes resulted in the precipitation of green solids, which were isolated on a medium porosity sintered glass frit. After washing with additional petroleum ether (3 x 10 mL), the green solids were dried under reduced pressure to yield **2.9** as a pure compound (0.090 g, 51 %). Crystals of **2.9** were grown via vapor diffusion of petroleum ether into a benzene solution. ^{1}H NMR (C_6D_6, 300 MHz): δ 13.7 (s); 13.3 (s); 11.3 (br, s); 9.92 (t, J = 6.0 Hz); 9.75 (br, s); 9.11 (t, J = 6.3 Hz); 5.43 (d, J = 6.3 Hz); 3.18 (t, J = 6.0 Hz); -0.70 (br, s). UV-vis (C_6H_6) λ, nm (ε, M^{-1} cm^{-1}): 639 (3400). Evans Method (C_6D_6): 1.88 μ_B.

Synthesis of [PhBP$_3$]Fe≡N(Ph-*p*-NMe$_2$), 2.10: Compound **2.4** (0.200 g, 0.199 mmol) was added to benzene (~5 mL) with stirring. A benzene solution (1 mL) of N_3(Ph-*p*-NMe$_2$) (0.0475 g, 0.399 mmol) was added dropwise, resulting in a rapid color change from orange to forest green. After 12 hours the reaction was concentrated to a volume of 2 mL under reduced pressure. The addition of petroleum ether (~18 mL) and stirring for an additional 30 minutes resulted in the precipitation of green solids, which were isolated on a medium porosity sintered glass frit. After washing with additional petroleum ether (3 x 10 mL), the green solids were dried under reduced pressure to yield **2.10** (0.119 g, 72 %) contaminated with traces of the phosphaimide byproduct as evidenced by ^{1}H and ^{31}P NMR spectroscopy. Crystallization of the crude solids via vapor diffusion of petroleum ether into benzene yielded pure 17 (0.050 g, 29 %). ^{1}H NMR (C_6D_6, 300 MHz): δ 17.1 (s); 12.8 (br, s); 10.5 (s); 9.70 (t, J = 6.0 Hz); 8.93 (t, J = 7.5 Hz); 6.00 (d, J = 6.0 Hz); 3.20 (s); 2.20 (br, s); -0.27 (br, s). UV-vis (C_6H_6) λ, nm (ε,

M^{-1} cm^{-1}): 446 (17000); 699 (6,500). Evans Method (C_6D_6): 1.80 μ_B. Anal. Calcd. for $C_{53}H_{51}BFeN_2P_3$: C, 72.70; H, 5.87; N, 3.20. Found: C, 72.90; H, 6.05; N, 3.22.

Synthesis of [PhBP$_3$]Fe≡N^{t}Bu, 2.11: Compound **2.4** (0.200 g, 0.199 mmol) was added to benzene (~5 mL) with stirring. A benzene solution (1 mL) of *tert*-butylazide (0.0395 g, 0.398 mmol) was added dropwise, during which time the reaction changed color from orange to brown. After 12 hours volatiles were removed under reduced pressure. The resulting crude solids were washed with petroleum ether (3 x 20 mL) and dried under reduced pressure to yield **2.11** as a brown solid (0.113 g, 70 %). X-ray quality crystals were grown via slow evaporation of a benzene solution. ^{1}H NMR (C_6D_6, 300 MHz): δ 19.3 (br, s); 16.5 (br, s); 15.0 (s); 10.6 (t, J = 3.0 Hz); 9.61 (t, J = 6.8 Hz); 4.92 (d, J = 6.6 Hz); 2.39 (t, J = 6.6 Hz); -3.67 (br, s). UV-vis (C_6H_6) λ, nm (ε, M^{-1} cm^{-1}): 418 (1300); 506 (830). Evans Method (C_6D_6): 1.96 μ_B. Anal. Calcd. for $C_{49}H_{50}BFeNP_3$: C, 72.43; H, 6.20; N, 1.72. Found: C, 72.26; H, 6.11; N, 1.83.

Synthesis of [PhBP$_3$]Fe≡N(1-Ad), 2.12: Compound **2.4** (0.100 g, 0.0996 mmol) was added to benzene (~5 mL) with stirring. A benzene solution (1 mL) of 1-azidoadamantane (0.0353 g, 0.199 mmol) was added dropwise, during which time the reaction changed color from orange to brown. After 12 hours volatiles were removed under reduced pressure. The resulting crude solids were washed with petroleum ether (3 x 20 mL) and dried under reduced pressure to yield **2.12** as a brown solid (0.071 g, 80 %). X-ray quality crystals were grown via vapor diffusion of petroleum ether into a benzene solution. ^{1}H NMR (C_6D_6, 300 MHz): δ 23.1 (br, s); 16.8 (br, s); 14.9 (s); 10.6 (t, J = 6.3 Hz); 9.61 (t, J = 7.2 Hz); 7.99 (d, J = 12.3 Hz); 6.50 (d, J = 11.1 Hz); 5.01 (d, J = 7.2 Hz); 3.48 (s); 2.48 (t, J = 6.3 Hz); -3.34 (br, s). UV-vis (C_6H_6) λ, nm (ε, M^{-1} cm^{-1}):

422 (1600); 510 (1050). Evans Method (C_6D_6): 1.98 μ_B. Anal. Calcd. for $C_{55}H_{56}BFeNP_3$: C, 74.17; H, 6.34; N, 1.57. Found: C, 74.13; H, 6.26; N, 1.72.

Synthesis of [PhBP$_3$]Fe(CO)$_2$, 2.13: A benzene solution (3 mL) of **2.4** (0.100 g, 0.0996 mmol) was pressurized with an atmosphere of CO. This resulted in a color change from yellow-orange to light brown. After 30 minutes at room temperature, volatiles were removed under reduced pressure, and the resulting tan solid was washed with petroleum ether (3 x 5 mL) and dried to yield **2.13** (0.0558 g, 70 %). X-ray quality crystals were grown from vapor diffusion of petroleum ether into a benzene solution. ^{1}H NMR (C_6D_6, 300 MHz): δ 8.97 (br, s); 8.39 (br, s); 7.88 (s); 7.67 (s); 7.38 (s); 7.03 (s); 4.71 (br, s). IR (C_6H_6): 1979, 1914 cm^{-1}. ES-MS: calcd. for $C_{47}H_{41}BFeO_2P_3$ $(M)^+$ 797 m/z, found $(M - 2\ CO)^+$ 741 m/z. Evans Method (C_6D_6): 1.73 μ_B. Anal. Calcd. for $C_{47}H_{41}BFeO_2P_3$: C, 70.79; H, 5.18. Found: C, 70.46; H, 4.96.

Synthesis of [PhBP$_3$]Fe(C≡N^{t}Bu)$_2$, 2.14: Compound **2.4** (0.100 g, 0.0996 mmol) was added to benzene (~5 mL) with stirring. A benzene solution (1 mL) of ^{t}BuN≡C (22.5 μL, 0.199 mmol) was added dropwise, during which time the reaction reddened in color. After 4 hours at room temperature, the reaction was concentrated under reduced pressure to a volume of ~ 2 mL. The addition of 15 mL of petroleum ether resulted in the precipitation of a red-orange solid that was isolated and dried to yield **2.14** (0.073 g, 81 %). X-ray quality crystals were grown from vapor diffusion of petroleum ether into a benzene solution. ^{1}H NMR (C_6D_6, 300 MHz): δ 9.08 (br, s); 8.28 (br, s); 7.80 (s); 7.56 (s); 4.26 (br, s); 2.23 (br, s). IR (C_6H_6): 2058, 2019 cm^{-1}. Evans Method (C_6D_6): 1.75 μ_B. Anal. Calcd. for $C_{55}H_{59}BFeN_2P_3$: C, 72.78; H, 6.55; N, 3.09 Found: C, 72.78; H, 6.39; N, 3.03.

Quantification of *p*-tolylisocyanate: A J. Young tube was charged with **2.5** (0.0107 g, 0.0126 mmol), hexamethylbenzene (0.0013 g, 0.0080 mmol), and C_6D_6 (~ 0.5 mL) under an atmosphere of N_2. The addition of an additional atmosphere of CO resulted in a color change from green to purple, and finally yellow-brown within minutes. After allowing the reaction to proceed at room temperature for 10 minutes, ^1H NMR integration versus the internal standard revealed that *p*-tolylisocyanate had been generated in approximately quantitative yield.

Reaction of 2.13 with *p*-tolylazide: An NMR tube was charged with **2.13** (0.0100 g, 0.0125 mmol), *p*-tolylazide (0.0033 g, 0.025 mmol), ferrocene (0.0017 g, 0.0091 mmol), and C_6D_6 (~ 1.5 mL). The reaction gradually (hours) turns forest green and after 44 hours at room temperature, integration versus the internal ferrocene reference revealed that *p*-tolylisocyanate had been generated in 80% yield. The paramagnetic metal-containing product was identified as **2.5**.

2.5.9 X-ray Experimental Data

X-ray diffraction studies were carried out in the Beckman Institute Crystallographic Facility on a Bruker Smart 1000 CCD diffractometer under a stream of dinitrogen. Data were collected using the Bruker SMART program, collecting ω scans at 5 ϕ settings. Data reduction was performed using Bruker SAINT v6.2. Structure solution and structure refinement were performed using SHELXS-97 (Sheldrick, 1990) and SHELXL-97 (Sheldrick, 1997). All structural representations were produced using the Diamond software program. Crystallographic data are summarized in Table 2.1.

Table 2.2. Crystallographic data for [PhBP$_3$]FeCl, **2.1**; [PhBP$_3$]Fe(PPh$_3$), **2.4**; [PhBP$_3$]Fe≡N-*p*-tolyl, **2.5**; [PhBP$_3$]FeN^{t}Bu, **2.11**; and [PhBP$_3$]Fe(CO)$_2$, **2.13**.

	2.1·C_6H_6	**2.4**·C_5H_{10}·0.5C_6H_6	**2.5**·0.5C_6H_6
chemical formula	$C_{51}H_{47}BClFeP_3$	$C_{71}H_{69}BFeP_4$	$C_{55}H_{51}BFeNP_3$
fw	854.91	1112.80	885.54
T (°C)	-177	-177	-177
λ (Å)	0.71073	0.71073	0.71073
a (Å)	10.9340(17)	20.2596(6)	10.9216(8)
b (Å)	16.666(3)	17.7356(6)	16.9009(13)
c (Å)	24.153(3)	33.4617(11)	25.2795(19)
α (°)	90	90	85.0390(10)
β (°)	102.752(13)	90	85.4520(10)
γ (°)	90	90	77.0040(10)
V (Å^3)	4292.8(11)	12023.3(7)	4521.0(6)
space group	P2(1)/c	Pbca	P-1
Z	4	8	4
D_{calc} (g/cm^3)	1.323	1.230	1.301
μ(cm^{-1})	5.61	3.99	4.79
R1, wR2[a] ($I > 2\sigma(I)$)	0.0467, 0.0746	0.0713, 0.1170	0.0497, 0.0704

[a] $R1 = \Sigma||F_o| - |F_c||/\Sigma|F_o|$, $wR2 = \{\Sigma[w(F_o^2 - F_c^2)^2]/\Sigma[w(F_o^2)^2]\}^{1/2}$

Table 2.2 cont.

	2.11	**2.13**
chemical formula	$C_{49}H_{50}BFeNP_3$	$C_{47}H_{41}BFeO_2P_3$
fw	812.47	797.37
T (°C)	-177	-177
λ (Å)	0.71073	0.71073
a (Å)	14.7124(13)	9.7323(9)
b (Å)	19.0114(17)	17.2050(15)
c (Å)	15.0887(13)	23.208(2)
α (°)	90	90
β (°)	96.9378(17)	95.718(2)
γ (°)	90	90
V (Å^3)	4189.5(6)	3866.8(6)
space group	P2(1)/n	P2(1)/n
Z	4	4
D_{calc} (g/cm^3)	1.288	1.370
μ(cm^{-1})	5.10	5.54
R1, wR2^a ($I > 2\sigma(I)$)	0.0429, 0.0848	0.0505, 0.0888

References Cited

---

[1] (a) Einsle, O.; Tezcan, A.; Andrade, S. L. A.; Schmid, B.; Yoshida, M.; Howard, J. B.; Rees, D. C. *Science* **2002**, *297*, 1696. (b) Rees, D. C. *Annu. Rev. Biochem.* **2002**, *71*, 221. (c) Peters, J. W.; Lanzilotta, W. N.; Lemon, B. J.; Seefeldt, L. C. *Science* **1998**, *282*, 1853.

[2] (a) Seyferth, D.; Henderson, R. S.; Song, L. C. *Organometallics* **1982**, *1*, 125. (b) Zhao, X.; Georgakaki, I. P.; Miller, M. L.; Mejia-Rodriguez, R.; Chiang, C. Y.; Darensbourg, M. Y. *Inorg. Chem.* **2002**, *41*, 3917. (c) Gloaguen, F.; Lawrence, J. D.; Schmidt, M.; Wilson, S. R.; Rauchfuss, T. B. *J. Am. Chem. Soc.* **2001**, *123*, 12518.

[3] See: Lappert, M. F.; MacQuitty, J. J.; Pye, P. L. *J. Chem. Soc., Dalton Trans.* **1998**, 1583 and references therein.

[4] Kisko, J. L.; Hascall, T.; Parkin, G. *J. Am. Chem. Soc.* **1998**, *120*, 10561.

[5] Thomas, J. C.; Peters, J. C. *Inorg. Synth.* **2004,** *34,* 8.

[6] (a) Rohde, J.-U.; In, J.-H.; Lim, M. H.; Brennessel, W. W.; Bukowski, M. R.; Stubna, A.; Münck, E.; Nam, W.; Que, L., Jr. *Science* **2003,** *299,* 1037. (b) MacBeth, C. E.; Golombek, A. P.; Young, V. G., Jr.; Yang, C.; Kuczera, K.; Hendrich, M. P.; Borovik, A. S. *Science* **2000**, *289*, 938. (c) Verma, A. K.; Nazif, T. N.; Achim, C.; Lee, S. C. *J. Am. Chem. Soc.* **2000**, *122*, 11013. (d) Que, L., Jr.; Chen, K.; Costas, M.; Ho, R. Y. N.; Jensen, M. P.; Rohde, J. U.; Torelli, S.; Zheng, H. *J. Inorg. Biochem.* **2001**, *86*, 88. (e) Pistorio, B. J.; Chang, C. J.; Nocera, D. G. *J. Am. Chem. Soc.* **2002**, *124*, 7884. (f) Tshuva, E. Y.; Lee, D.; Bu, W.; Lippard, S. J. *J. Am. Chem. Soc.* **2002**, *124*, 2416. (g) Meunier, B., Ed. *Biomimetic Oxidations Catalyzed by Transition Metal Complexes*; Imperial College Press: London, 2000.

---

[7] Mansuy and co-workers were the first to report heme-supported $[FeNNR_2]^+$ systems. Physical data for these systems suggests they are better represented as Fe(II) $[Fe \leftarrow NNR_2]$. See: Mansuy, D.; Battioni, P.; Mahy, J. P. *J. Am. Chem. Soc.* **1992,** *104,* 4487.

[8] Wieghardt and Meyer have provided spectroscopic evidence at 77 K for an Fe(V) nitride. See: Meyer, K.; Bill, E.; Weyhermuller, T.; Wieghardt, K. *J. Am. Chem. Soc.* **1999**, *121,* 4859.

[9] Shapiro, I. R.; Jenkins, D. M.; Thomas, J. C.; Day, M. W.; Peters, J. C. *Chem. Commun.* **2001**, 2152.

[10] (a) Sur, S. K. *J. Magn. Reson*. **1989**, *82*, 169. (b) Evans, D. F. *J. Chem. Soc*. **1959**, 2003.

[11] Miessler, L. G.; Tarr, D. A. *Inorganic Chemistry,* 2nd Ed.; Prentice Hall: New Jersey, 1999; pg. 343.

[12] Jenkins, D. M.; Di Bilio, A. J.; Allen, M. J.; Betley, T. A.; Peters, J. C. *J. Am. Chem. Soc.* **2002,** *124,* 15336.

[13] Betley, T. A.; Peters, J. C. *Inorg. Chem.* **2003,** *42,* 5074.

[14] Trofimenko, S. *Scorpionates: Polyporazolylborate Ligands and Their Coordination Chemistry;* Imperial College Press: London, 1999.

[15] (a) Ohrenberg, C.; Ge, P.; Schebler, P.; Riordan, C. G.; Yap, G. P. A.; Rheingold, A. L. *Inorg. Chem.* **1996,** *35,* 749. (b) Ge, P.; Haggerty, B. S.; Rheingold, A. L.; Riordan, C. G. *J. Am. Chem. Soc.* **1994,** *116,* 8406.

[16] See for example: Dapporto, P.; Midollini, S.; Sacconi, L. *Inorg. Chem.* **1975,** *14,* 1643.

[17] See for example: (a) Shirasawa, N.; Nguyet, T. T.; Hikichi, S.; Moro-oka, Y.; Akita, M. *Organometallics* **2001,** *20,* 3582. (b) Ito, M.; Amagai, H.; Fukui, H.; Kitajima, N.;

Moro-oka, Y. *Bull. Chem. Soc. Jpn.* **1996,** *69,* 1937. (c) Gorrell, I. B.; Parkin, G. *Inorg. Chem.* **1990,** *29,* 2452. (d) Brunker, T. J.; Hascall, T.; Cowley, A.R.; Rees, L. H.; O'Hare, D. Inorg. Chem. **2001,** *40,* 3170.

[18] The reduction of $[PhB^{iPr}_3]FeCl$ with a sodium/mercury amalgam under a dinitrogen atmosphere results in the formation of the Fe^{I}-N_2 dimer, $([PhB^{iPr}_3]Fe)_2(\mu\text{-}N_2)$. See: Betley, T. A.; Peters, J. C. *J. Am. Chem. Soc.* **2003,** *125,* 10782.

[19] For example, $[PhBP_3]Fe(N(H)\text{-}p\text{-tolyl})$ features an Fe-N bond length of 1.9132(18) Å. See Chapter 3.

[20] Kahn, O. *Molecular Magnetism;* VCH Publishers: New York, 1993; Ch. 2.

[21] Spin-crossover has been observed in a number of $[PhBP_3]Co(II)$ systems. See: (a) Jenkins, D. M.; Peters, J. C. *J. Am. Chem. Soc.* **2003,** *125,* 11162. (b) Jenkins, D. M.; Peters, J. C. *J. Am. Chem. Soc.* In Press.

[22] See Section 2.3 for a DFT study of $[PhBP_3]Fe\equiv N^tBu$.

[23] Jenkins, D. M.; Betley, T. A.; Peters, J. C. *J. Am. Chem. Soc*. **2002**, *124*, 11238.

[24] See Chapter 4 for a comparative structural study between terminal d^5 and d^6 iron imides supported by $[PhBP_3]$.

[25] Terminal cobalt trimethylsilyl imido species have been inferred as intermediates in ligand activation processes. See: Thyagarajan, S.; Shay, D. T.; Incarvito, C. D.; Rheingold, A. L.; Theopold, K. H. *J. Am. Chem. Soc.* **2003,** *125,* 4440.

[26] Glueck, D. S.; Wu, J.; Hollander, F. J.; Bergman, R. G. *J. Am. Chem. Soc.* **1991,** *113,* 2041.

[27] Mindiola, D. J.; Hillhouse, G. L. *J. Am. Chem. Soc.* **2001**, *123*, 4623.

---

[28] Jenkins, D. M. *Low spin pseudotetrahedral cobalt(trisphosphino)borate complexes*, Caltech, Ph.D. Thesis, 2005.

[29] See for example: (a) Bach, T.; Körber, C. *Eur. J. Org. Chem.* **1999,** 1033. (b) Mahy, J.-P.; Battioni, P.; Mansuy, D. *J. Am. Chem. Soc.* **1986,** *108,* 1079.

[30] Ertl, G. In *Catalytic Ammonia Synthesis: Fundamentals and Practice;* Jennings, J. R.; Ed.; Plenum Press: New York, 1991; pp 109-132.

[31] Mehn, M. P.; Jensen, M. P.; Que, L., Jr.; Brown, S. D.; Jenkins, D. M.; Betley, T. A.; Peters, J. C. *Manuscript in Preparation.*

[32] (a) Mukherjee, A.; McGlashen, M. L.; Spiro, T. G. *J. Chem. Phys.* **1995,** *99,* 4912. (b) Varsanyi, G. *Vibrational Spectra of Benzene Derivatives;* Academic Press: New York, 1969.

[33] Synthetic protocols afford 50% ^{15}N incorporation. See Section 2.5.7.

[34] Osborne, J. H.; Trogler, W. C. *Inorg. Chem.* **1985,** *24,* 3098.

[35] Mindiola, D. J.; Hillhouse, G. L. *Chem. Commun.* **2002**, 1840.

[36] Waterman, R.; Hillhouse, G. L. *J. Am. Chem. Soc.* **2003,** *125,* 13350.

[37] For examples of five-coordinate, bridging iron(III) imides see: Nichols, P. J.; Fallon, G. D.; Murray, K. S.; West, B. O. *Inorg. Chem.* **1988,** *27,* 2795.

[38] Feldman, J. D.; Peters, J. C.; Tilley, T. D. *Organometallics* **2002,** *21,* 4050.

[39] See for example: (a) Reinaud, O. M.; Rheingold, A. L.; Theopold, K. H. *Inorg. Chem.* **1994,** *33,* 2306. (b) Rheingold, A. L.; Liable-Sands, L. M.; Golen, J. A.; Yap, G. P. A.; Trofimenko, S. *Dalton Trans.* **2004,** 598.

[40] Curiously, $[PhBP^{iPr}_3]CoI$ features a high-spin electronic configuration in contrast to the low-spin configuration observed for $[PhBP^{iPr}_3]CoI$. This is counter intuitive for an

---

assumed stronger-field ligand, and one working hypothesis suggests that with bulky alkyl groups, the second generation tris(phosphino)borate is not able to distort to accommodate a Jahn-Teller distortion. See reference [13].

[41] See for example: (a) Cundari, T. R. *J. Am. Chem. Soc.* **1992,** *114,* 7879. (b) Mayer, J. M. *Comments Inorg. Chem.* **1988,** *8,* 125. (c) Osborne, J. H.; Rheingold, A. L.; Trogler, W. C. *J. Am. Chem. Soc.* **1985,** *107,* 7945. (d) Nugent, W. A. *Coord. Chem. Rev.* **1980,** *31,* 123.

[42] Albright, T. A.; Burdett, J. K.; Whangbo, M.-H. *Orbital Interactions in Chemistry;* Wiley-Interscience: New York, 1985; pp 387-389.

[43] A DFT study with the closed-shell system $\{[PhBP_3]Fe{\equiv}N^tBu\}^-$ yields a HOMO-LUMO gap of 86 kcal/mol. See Chapter 4.

[44] Betley, T. A.; Peters, J. C. *J. Am. Chem. Soc.* **2004,** *126,* 6252.

[45] For structurally characterized terminal iron oxos see references [6a] and [6b].

[46] Wagner, W. D.; Nakamoto, K. *J. Am. Chem. Soc.* **1988,** *110,* 4044.

[47] For a detailed vibrational analysis of niobium and tantalum arylamido systems see: Heinselman, K. S.; Miskowski, V. M.; Geib, S. J.; Wang, L. C.; Hopkins, M. D. *Inorg. Chem.* **1997,** *36,* 5530.

[48] Jaguar 5.0, Schrodinger, LLC, Portland, Oregon, 2002.

[49] Lee, C.; Yang, W.; Parr R. G. *Phys. Rev. B* **1988**, *37*, 785.

[50] Smith, P. A. S.; Brown, B. B. *J. Am. Chem. Soc.* **1951,** *73,* 2438.

[51] Abramovitch, R. A.; Challand, S. R.; Scriven, E. F. V. *J. Org. Chem.* **1972,** *37,* 2705.

[52] (a) Li, Y.; Kirby, J. P.; George, M. W.; Poliakoff, M.; Schuster, G. B. *J. Am. Chem. Soc.* **1988,** *110,* 8092. (b) Smith, P. A. S.; Hall, J. H. *J. Am. Chem. Soc.* **1962,** *84,* 480.

---

[53] Bottaro, J. C.; Penwell, P. E.; Schmitt, R. J. *Syn. Comm.* **1997,** *27,* 1465.

[54] Crivello, J. V. *J. Org. Chem.* **1981,** *46,* 3056.